The aerodynamic design of RED Shift

Solar Team Twente's 7th solar car

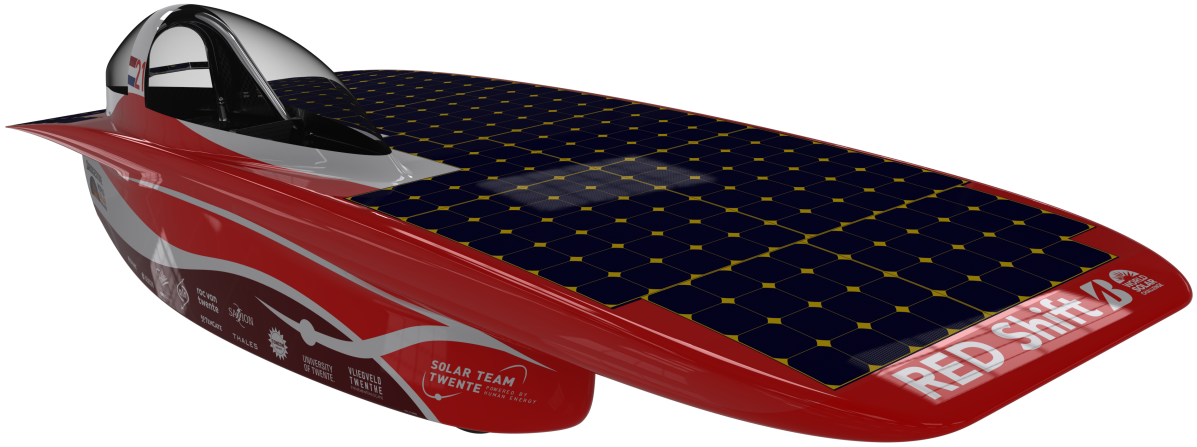

Author:
Luc Evertzen

Supervisor UT:
Prof. Dr. Ir. A. de Boer

Applied Mechanics
Faculty of Engineering Technology,
University of Twente
P.O. Box 217
7500 AE Enschede
The Netherlands

Supervisor NLR:
Ir. J.E.J. Maseland

NLR Amsterdam
Anthony Fokkerweg 2
1059 CM Amsterdam
The Netherlands

Basic Information

Student

Name	Luc Evertzen
Student number	s1380400
Study	Mechanical Engineering
	Research & Development
	Mechanics of Solids, Surfaces & Systems

University

Name	University of Twente
Department	Applied Mechanics
Faculty	Faculty of Engineering Technology
Mentor	Prof. Dr. Ir. André de Boer

Company

Name	Solar Team Twente
Department	Aerodynamics
Mentor	Ir. Hans Maseland
City	Enschede
Country	The Netherlands

Internship

Title Assignment	The aerodynamic design of RED Shift
	Solar Team Twente's 7^{th} solar car
Period	Sep. 2016 - Nov. 2017

Abstract

keywords: ***aerodynamics, cfd, cad, windtunnel, banked road, solar car, solar team twente***

This report describes the aerodynamic development of Solar Team Twente's 7th solar car, RED shift. It encompasses all design phases of the solar car and includes conceptual design, computer aided design & computational fluid dynamics, windtunnel tests and various banked road tests. For the 2017 edition the solar array area was reduced to 4 m^2 from 6 m^2 and a number of stricter safety regulations were added concerning the driver's occupant space.

The previous team also had various recommendations regarding aerodynamic improvements to the car. This concerned the boundary layer diverters of the wheel fairings, the canopy design, the track width and wheel base, wheel casing improvements and various other aspects of the design of the car.

The main recommendation to the 2018 team is to spend more time on the conceptual design. Trends should be identified in order to arrive at a more global optimum. A new trade off study should be performed regarding the solar arrays and a more detailed analysis of track width/wheel base configurations and wheel fairing positioning should be performed. For the theoretical design, an analysis of rotating wheels will be of great importance to key aerodynamic features of the solar car. Building an isolated test-setup for the windtunnel which can validate these theoretical analyses will also be key. Improvements can also be made to the banked road tests, both the velocity correction necessary due to the presence of wind and the final fitting of the data to obtain the correct C_dA should be considered.

Table of Contents

1. Introduction

The Challenge

The Bridgestone World Solar Challenge (BWSC) [1] is a biennial engineering challenge which requires teams to travel from Darwin to Adelaide on nothing else but solar power. The challenge includes two competitive classes: The Cruiser class and the Challenger class. The aim of the Cruiser class is to design solar powered vehicles which keep practicality and day-to-day use in mind. They are road legal vehicles designed to transport multiple people in relative comfort. Solar Team Twente does not compete in this class, so it will not be discussed further. The other class is the Challenger class. The aim of the Challenger class is to design a car which will travel from Darwin to Adelaide as efficient and as fast as possible. Solar Team Twente has been competing in this class ever since their initial participation in 2005.

Figure 1: The route map of the 2017 BWSC

The challenge officially starts at the Hidden Valley Raceway in Darwin, where each team drives a qualifying lap which will determine the starting grid for the challenge. From the town hall in Darwin the route mostly follows the Stuart Highway for a total of approximately 3000 km. Competitors are allowed to race from 0800 until 1700 and camp in the outback in between race days. Ten control stops have been set up along the race route, see Figure 1. When competitors arrive at these control stops they will have to switch drivers and also leave the car stationary for a full 30 minutes before continuing.

The Regulations

The rules for the 2017 BWSC [2] were released on the 22nd of April 2016. These rules incorporated one of the most drastic rule changes in the history of the challenge. Besides modifications to the rules designed to improve safety or patch certain loopholes, the most notable change was the reduction in allowable solar array area. The allowed area was reduced from 6 m^2 to 4 m^2. As one can imagine the size of the solar array is one of the key features for the aerodynamic design of the solar car. This implied a complete redesign for the aerodynamics of the 2017 solar car.

> 2.4.2 If the solar collector comprises photo-voltaic cells all of the same chemistry and used without concentrators such as reflectors or lenses then the total cell area, found by summing the exposed surface areas of the component photo-voltaic cells, must not exceed the allowable total cell area (of 4 m^2 for Si arrays).

The other big set of modifications to the rules regarded the safety and visibility demands of the occupant of the solar car. Extra head clearance around the occupant's helmet and increased forward visibility

demands required a complete redesign of the canopy, which is one of the key features of the solar car and one of the most challenging design aspects to correctly implement.

2.11.4	No point of any occupant's helmet may lie within 50 mm of the convex hull.

2.17.1	Each driver, when seated in the normal driving position with safety-belt and helmet on, must be able to identify 75 mm high letters at every point of forward travel that is: • 4 m from the driver's eyes, and • between 0.4 m below eye level and 0.7 m above eye level, and • between 100^{o} left and 100^{o} right of the direction of travel.

The Project

The entire project consists of multiple phases, not all of which are related to the theoretical design of the solar car. It is therefore useful to lay out a rough idea of the planning of the project and the different phases that the project goes through.

The project starts off in September with the theoretical design phase of the project. During this phase most theoretical aspects of the solar car design are done. This includes all mechanical, structural and aerodynamic design carried out for the car. For the aerodynamics team this phase consists of multiple sub-phases. In the first phase the pre-design of the car is done. In this phase the general configuration of the solar car is designed. The phase concludes with a conceptual design review, after which the detailed design of the solar car is started. A preliminary design review adds a final check to the theoretical phase, after which the final design is fine-tuned. This phase lasts until the end of January, when focus is shifted to testing and production. During most of February all mechanical and electrical components will be tested on a mock-up frame of the solar car to check for any design flaws before applying the parts on the actual solar car.

During the months after February focus is shifted mostly to the structural and mechanical production of the solar car, with two big exceptions for the aerodynamics team. The first is the windtunnel test, in which the aerodynamics team travels to NLR's (Netherlands Aerospace Centre)/DNW's (German-Dutch Wind Tunnels) windtunnel for verifying the Computational Fluid Dynamics (CFD) analyses and for testing as much practical aerodynamic aspects as possible in a controlled environment. The second major exception are the two weekends spend at RDW's (governmental organization for the registration of road vehicles) banked road together with the electrical engineers, strategist and data acquisist to further analyze the real world aerodynamic performance of the solar car.

The last phase in The Netherlands encapsulates the final on-road testing of the solar car. This phase is mostly used for further testing of electrical and data acquisition components in the solar car and for perfecting any communication protocols and procedural agreements necessary during the race. During this phase and any subsequent phases, the aerodynamic design is not further optimized, as focus is shifted to other important aspects of the project.

After travelling to Australia there is one final phase which is crucial to the performance of the solar car, which is the on road testing of the solar car in Australia. This phase is the final testing phase in which any problems (Australia specific or not) can be found and remedied before the start of the race.

Hans Maseland

Hans Maseland is a Research Engineer at NLR, the Dutch aerospace research institute. He provided us with feedback during my time at Solar Team Twente. There is virtually no part of the aerodynamic

design where Hans did not help us with techniques, insights and tips. From analysis techniques like the C_p plots, turbulent kinetic energy and total pressure losses to design tips like cutting off the trailing edge of the canopy and the boundary layer diverters.

NLR will again be involved in the team's 2019 effort to secure the BWSC title and Hans will also return to provide guidance to the new aerodynamic team of Solar Team Twente. Hans was an invaluable addition to the team's 2017 effort and it is recommended that this cooperation will continue with the 2019 team.

2. Problem Definition

The regulations of the BWSC change. As a consequence, all teams have to update their design in order to comply to the new regulations. Not only to improve on their previous designs, but also to stay compliant to the rules. For most editions the rules do not change much. The 2017 edition of the Bridgestone World Solar Challenge was different. Teams were only allowed to race with two thirds of the solar array area they used previously. So apart from any improvements and updates moving on from 2015 the 2017 teams also had to make sure they complied to this drastic rule change. Below the problem definition has been split into two main parts. The first part consists of a brief description of all the recommendations made by the 2015 team. The second part lists all changes and improvements that had to be made in order to comply to the new set of regulations.

Recommendations after 2015

Figure 2: The 2015 contender of Solar Team Twente, Red One

All recommendations issued by the 2015 team were provided without the knowledge of the drastic rule changes to come. They did not neglect the rule change in their advise, the changes simply were not known at the time. Their advise was focused on improving upon the 2015 contender, Red One, shown in Figure 2.

The main advise of the 2015 team pointed at several aspects of the wheel fairings and the canopy. The first advise was to redesign the fillets of both the wheel fairings and the canopy. The fillet is the curved part of the body which connects the wheel fairing's leading edge to the main body. Mainly, to allow to boundary layer on the main body to be minimally disturbed by the presence of the wheel fairing while simultaneously aiding a smooth transition of the boundary layer of the main body onto that of the wheel fairing's leading edge and the wheel fairing in general. The same holds true for the fillet in front of the canopy. For Red One, the boundary layer on the main body was affected too much by the wheel fairings and canopy and the transition of the flow onto the fairings and canopy was not as good as it could have been, as can be seen in Figure 3a. Figure 3a also shows that transition occurs almost immediately on the outside of the wheel fairings due to the non-optimal fillet not being able to divert the airflow properly.

Further issues arose in the general design of the small left wheel fairings because of the choice of two separate wheel fairings instead of a single longer one. A certain distance between both left wheel fairings was preferable to minimize the influence of the wake of the front wheel fairing on the downstream one. This resulted in a short chord design for both wheel fairings. The short chord design in turn resulted in a relatively steep adverse pressure gradient towards the rear of both wheel fairings. Unwanted flow

characteristics followed from the adverse pressure gradient, such as an area of recirculating flow on the front left wheel fairing, shown in Figure 3b.

A final aspect of the wheel fairings which could not be fully explored during the 2015 effort was the orientation of the wheel fairings. Because of the pressure difference between the bottom and the top of the solar car, the fluid flow does not approach the leading edge of the wheel fairings parallel to the direction of travel. Instead it approaches the leading edges of the wheel fairings at an outward angle due to the pressure difference under and above the main airfoil.

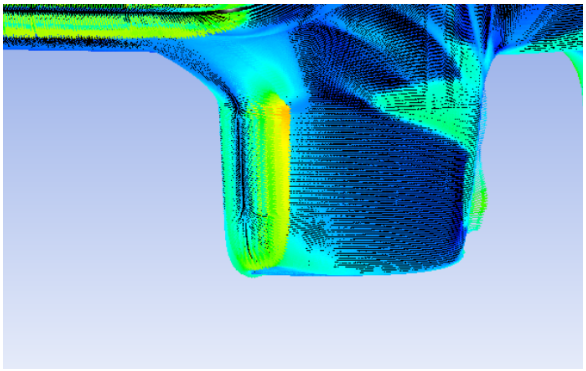

(a) The left front wheel fairing of the 2015 contender with skin friction plotted on the surface.

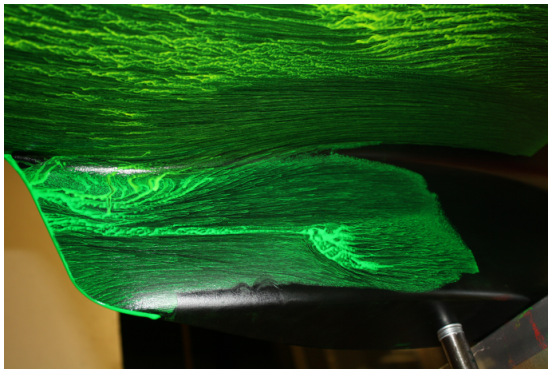

(b) Flow-viz results of the scale model windtunnel experiments

Figure 3: 2015 Wheel fairing issues

The 2015 team found out that the flow patterns on the left and right side of the canopy were not identical. This is caused by the interference of the main body boundary layer on the left side of the canopy, which slows down the airflow on that side of the canopy. This loss of energy makes it harder for the boundary layer on the left side of the canopy to overcome the adverse pressure gradient causing transition, and in the worst case flow separation, to occur earlier than expected. Previous teams tried to overcome this issue, but were mostly hindered by a lack of time and resources to truly tackle the problem. The main advise of the 2015 team was to redo the entire canopy if time permitted it, which later appeared to be a necessity due to changes in the regulations, as discussed in Section 2.2. At the very least a certain amount of trailing edge twist had to be added to the canopy to account for the asymmetric airflow around it.

In order to be able to make all these changes, a new surface modeling tool was required. The 2017 aerodynamics team switched from SolidWorks [3] to Rhinoceros 3D [4], which is a dedicated surface modeling tool better suited to creating aerodynamic models for CFD analyses.

(a) The wheel casing design of 2015

(b) The wheel casing design of a 2015 competitor

Figure 4: Various wheel casing designs

The 2015 aerodynamics team introduced special wheel casings, which reduced the amount of rotating wheel exposed to the surrounding flow. They are shown in Figures 4a and 4b. This significantly reduced the amount of pressure drag caused by the wheels, which was a large part of the total aerodynamic drag. They urged us to improve upon their design implementation. This included a better casing design, but also a better method to seal of the openings through which the wheels protrude.

The final advise the 2015 team left us with were related to the windtunnel tests and banked road tests. They recommended doing a full scale windtunnel test on the actual car, since the scale model used in previous years had reached its limits of usefulness for windtunnel analyses. The windtunnel test had mostly been used to validite the CFD model, but that model had not been significantly changed since then so verifying it again would be a waste of time and resources. Instead they told us to focus mostly on any practical aspects of the aerodynamics of the solar car. To what extent was there a laminar boundary layer present on the vehicle? What effect did the split lines in between different body panels have on the transition from a laminar to a turbulent boundary layer? We would later add various extra research to our windtunnel test, which will be discussed in 6.

Regulatory demands for 2017

As mentioned earlier the regulations for the 2017 Bridgestone World Solar Challenge saw a radical change. The change in regulations concerned a reduction of the allowable solar array area from 6 m^2 to 4 m^2. This large reduction in solar panel area could be translated into a reduction in wheelbase, track width or both. The decision between two or one left wheel fairing(s) was wide open again and also the integration of the wheel fairings would have to be considered once more.

The second major change in the regulations regarded the occupant space and the safety demands regarding that occupant space. A new rule was introduced which demanded a larger clearance around the driver's head for improved safety in case of a roll. The rule is best explained as follows: Draw planes between the main structural parts of the body. Now draw a 50 mm offset from the driver's head in a normal driving position. The drawn planes and the 50 mm offset may not intersect. These planes are illustrated in Figures 5a and 5b. A canopy redesign was necessary in order to encapsulate the larger rollbar.

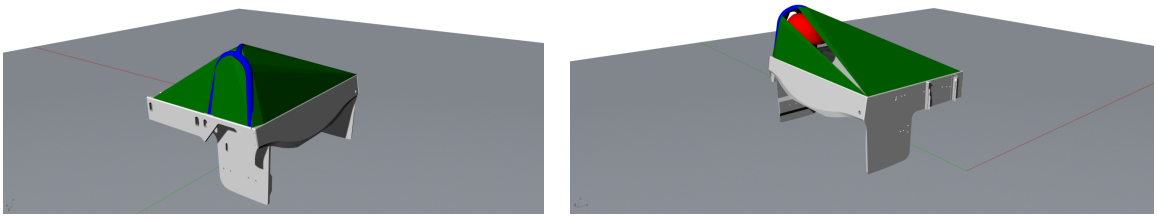

(a) Planes drawn for the rollbar to the ribs

(b) The offset of the helmet shown within the planes, not intersecting them

Figure 5: Extra room to meet the new safety standards set by the organization

2.11.4 No point of any occupant's helmet may lie within 50 mm of the convex hull.

3. Initial Design Considerations

The report will be split into three main parts. The first part will discuss the initial design considerations. This section will not go too in depth, but the decisions made here should be mentioned as they did influence the final design of the solar car. The second part will go in depth on the theoretical design aspects of the solar car. The last part will go into the practical aspects of designing a solar, which will include the windtunnel tests and the banked road tests.

Baseline airfoil shapes

The NACA series airfoils have been around since the 1930s [5]. The original set of airfoils was the 4-series, which described a set of standardized airfoil shapes with different thicknesses and camber lines. This series was later expanded into the 5-series [6], which allowed for more complex airfoil shapes. A specialized airfoil series was released which was designed to maximize the laminar flow over the airfoil. This series was called the 6-series [7] and is what was used as a basis for all the airfoil shapes used in the solar car. For the design of the solar car, minimizing the aerodynamic drag has the highest priority. The airfoil is described using multiple digits (i.e. NACA 61-315) in the following sequence:

1. The first digit is always a 6, which indicates the series.
2. Describes the distance of the minimum pressure area in tens of percent of chord.
3. The design lift coefficient in tenths.
4. Two digits indicating the maximum thickness in percentage of chord.

Various standard 6-series airfoils were initially analyzed using XFOIL [8]. Aerodynamic characteristics were analyzed and shape modifications were made using XFLR5 [9] to perfectly fit their use in the solar car. The C_p distribution of the airfoil was optimized to maximize laminar flow region. The C_p-plot of the main airfoil (2D representation) is shown in Figure 6. Several factors can be analyzed using just the C_p plot, without the need for a 3D design of the entire solar car. The pressure difference between the bottom and the top of the airfoil indicates the amount of lift generated by the airfoil. The start of the adverse pressure gradient is also visible, which gives an indication of the location of transition from a laminar to a turbulent boundary layer. The Reynolds number, lift coefficient, drag coefficient and lift/drag ratio are also calculated. Most 3D disturbances were counteracted with three dimensional aerodynamic design, which will be discussed in Section 5.

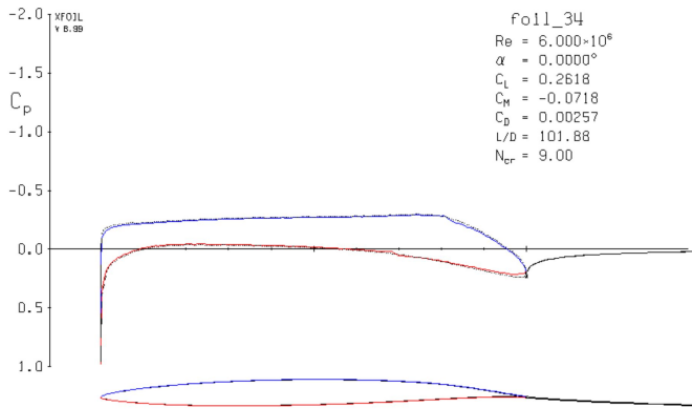

Figure 6: The C_p distribution of the final main airfoil used in the solar car.

Solar cell selection

One of the first decisions made in the project was the choice regarding the solar cell chemistry's. The organization left us with a choice of three solar cell chemistry's:

> 2.4.2 If the solar collector comprises photo-voltaic cells all of the same chemistry and used without concentrators such as reflectors or lenses then the total cell area, found by summing the exposed surface areas of the component photo-voltaic cells, must not exceed the allowable total cell area (of 4 m^2 for Si arrays).

Class	PV Cell Chemistry	Allowable total Cell Area (m^2)
Challenger	Si	4.000
	Multijunction GaAs	2.640
	Thin film GaAs	3.560
Cruiser	Si	5.000
	Thin film GaAs	4.440
	Multijunction GaAs	3.300

The decision was not limited to the aerodynamics subteam, the electrical team was also involved. Many parameters were compared in order to come to a final decision. While both Si and multijunction GaAs (simply GaAs from now on) had clear advantages, the single junction GaAs cells were not advantageous regarding power generation or wetted area. The two remaining chemistry's were compared in the following parameters:

- Income relative to temperature
- Angular radiance efficiency
- Solar intensity
- Efficiency solar cell
- Skin friction drag

For the sake of brevity, the electrical parameters will not be discussed in detail here, instead the conclusion will quickly be noted. Taking all the aforementioned factors into account excluding the difference in skin friction drag, the following comparison between different efficiency's Si and GaAs could be made (Table 1).

Table 1: A performance comparison between Si and GaAs solar arrays for different electrical efficiency's. A ratio above one is in favour of a GaAs array.

GaAs efficiency	Si efficiency	Ratio GaAs/Si
36	24.28	1.0181
34	24.28	0.9742
36	22	1.0696

The wetted area per solar array was also approximated. And was found to be approximately 17 m^2 for a catamaran with a Si array and approximately 14.5 m^2 for a catamaran with a GaAs array. Taking the wetted into account the new balance is listed in Table 2.

It can be seen that in all comparisons, the GaAs arrays are now more favourable than Si arrays. There was one major drawback to the GaAs array, which was its €200.000,- price tag. Or, in the case of 36% arrays, closer to €600.000,-. The budget of Solar Team Twente did not allow for such expenditures. So the GaAs concept had to be discarded and the Si concept was selected.

Table 2: A performance comparison between Si and GaAs solar arrays for differing efficiency's. A ratio above one is in favour of a GaAs array. Aerodynamics are now taken into account.

Scenario	**Effect EL**	**Effect Aero**	$\triangle$**t**
1. 34% GaAs vs 24% Si	0.974 (-21 min)	1.064 (46 min)	25.52 min
2. 35% GaAs vs 24% Si	1.018 (15 min)	1.064 (46n min)	61.16 min
3. 36% GaAs vs 22% Si	1.069 (54 min)	1.0696 (46 min)	100 min

Wheel base & Track width

Since the total solar array area decreased from 6m^2 to 4m^2, the solar car's main dimensions would be guaranteed to be smaller. The decrease in array area could either result in a decrease in wheel base or a decrease in track width, or a combination of both. RED One (Figure 2) used two wheel fairings on the left side of the solar car. A decrease in wheel base length would mean that the rear left wheel fairing would start to be negatively affected by the wake of the front left wheel fairing. A decrease in the wheel base would result in one long wheel fairing being used on the left side of the solar car, similar to the right side of the solar car. Depending on the wheel base and track width, different suspension setups would also be necessary, as not all suspension setups would fit for all cases. It was expected that narrowing the track width would affect the cornering stability of the car.

Usually, for 3D wings, a large aspect ratio ($width/length$) is preferable. The pressure difference below and above the wing introduces a vortical structure at the wing tip, which in turn leads to induced drag [10]. Having a high aspect ratio reduces the amount of induced drag per unit of lift, which is generally considereda as a good characteristic.

The solar car is not meant to be a lift generating device. The main design requirement for a solar car is minimizing drag. It was hypothesized that reducing the frontal area of the solar car would be a key factor in reducing the total drag of the solar car (keeping all other factors the same). The absolute lower bound for the track width of the solar vehicle was set at 900mm. This was not an aerodynamic consideration, but a direct result of the regulations of the BWSC:

> 2.17.1 Each driver, when seated in the normal driving position with safety-belt and helmet on, must be able to identify 75 mm high letters at every point of forward travel that is:
>
> - 4 m from the driver's eyes, and
> - between 0.4 m below eye level and 0.7 m above eye level, and
> - between 100º left and 100º right of the direction of travel.

This rule is probably hard to visualize, so Figure 7 gives a 3D representation of the frontal vision requirement which was used during the design of the 2017 solar car. Since a 4m^2 solar array will have to be fitted, a smaller track width results in a longer wheel base, which in turn results in a longer nose. Using this CAD representation of the frontal vision demand, 900mm was found to be the minimum track width of the solar car. A smaller track width would have resulted in a forward extended nose design which intersected with the frontal vision demand and would violate the requirements.

Two rudimentary designs were created for the trade-off study for the 900mm and 1000mm track width variants where everything was kept identical except for the track width. The key aerodynamic performance results are listed in Table 3. The 1000mm design has a much higher value for the shear drag, mostly due to its larger leading edge, where the skin friction is relatively high. The effect of the leading edge on the shear drag is illustrated in Figure 8.

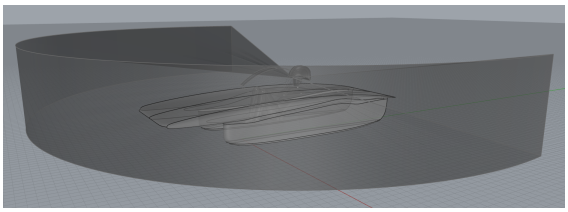

(a) The frontal vision demand as seen from the front

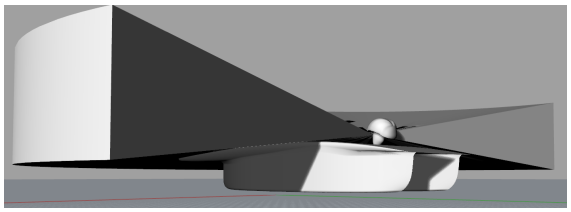

(b) The frontal vision demand as seen from the rear

Figure 7: The frontal vision demands set by the BWSC translated into a CAD model.

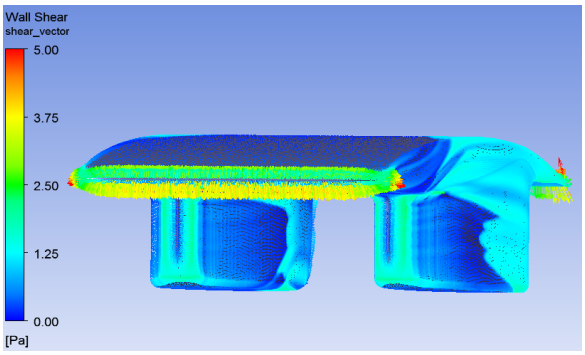

(a) The 900mm track width model as seen from the front

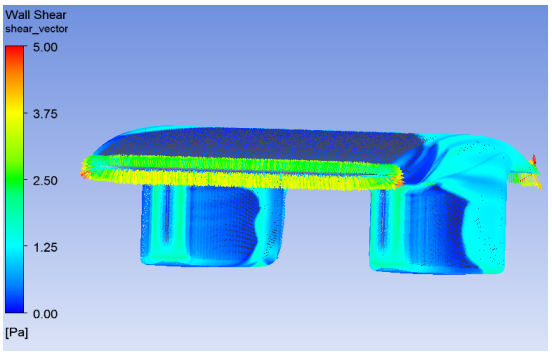

(b) The 1000mm track width model as seen from the front

Figure 8: A comparison between a 900mm track width and 1000mm track width variant of the solar car.

Table 3: The results for the 900mm and 1000mm track width versions

Version	**Wetted Area (m^2)**	C_dA	$C_{d,p}$	$C_{d,s}$	**Downforce (N)**
900mm	15.56	0.0460	0.0112	0.0349	29.9
1000mm	15.55	0.0503	0.0123	0.0382	26.7

The Venturi effect refers to the increase in fluid speed due to a decrease of the cross sectional area in confined flows. It was clear that, if the venturi effect could be managed for the 900mm case, the narrower track width concept did have a much lower shear drag and was therefore preferable. The next step was to determine the wheel base of the solar car. RED One employed a 2100mm wheel base, which resulted in the multiple wheel fairing design. This wheel base distance was chosen to both accommodate the larger solar array which was used in the 2015 edition of the BWSC and also for straight line stability. Even with a 900mm track width, a 2100mm wheel base was not necessary to accommodate the $4m^2$ array. It was also found that the car would still maintain its straight line stability at a wheel base of 1800mm (beyond the scope of this report). The driver could just fit in between the wheels at this track width as well, so an 1800mm wheel base was chosen.

As mentioned in the *Recommendations after 2015* section the short chord left wheel fairings were slightly controversial. Not only were they not feasible for a wheel base under approximately 2100mm, the width/chord ratio also resulted in a very steep adverse pressure gradient. This resulted in local air flow separation that has to be considered as detrimental. Since the new solar car would run a wheel base of 1800mm, the separate wheel fairing idea was dropped in favour of one large wheel fairing (similar to the right wheel fairing).

Spatial budgets

In order to have a baseline for the aerodynamic shape of the solar car spatial budgets are created. These range from suspension budgets, to driver budgets, to demands set by the organization.

The driver

The organization has several demands regarding the driver's orientation:

2.11.4	No point of any occupant's helmet may lie within 50 mm of the convex hull.
2.12.2	Each solar car occupant must have a seat that faces forward at an angle less than 10°, about a vertical axis, from the forward direction of travel.
2.12.4	Each occupant's heels must be below their hip point.
2.12.5	The angle between each occupant's shoulders, hips and knees must be more than 90°.
2.13.1	Occupant space for each seat must comply with Section LK of the Australian National Code of Practice for Light Vehicle Construction and Modification, as shown in the following diagram. The 835 mm radius arm must be able to move 45° forwards, 25° backwards and 7° either side of vertical. The solar car structure, including the windscreen, must lie wholly outside the occupant space. The steering wheel, mirrors, seat backs and head restraints may be inside the occupant space, but must be designed to minimize the risk of injury in a crash.

These demands were converted to a 3D model of the driver and the occupant space as defined by the organization, shown in Figure 9. The model was subsequently used for the right wheel fairing, the canopy and the determination of the wheelbase and the spatial budgets of the suspension.

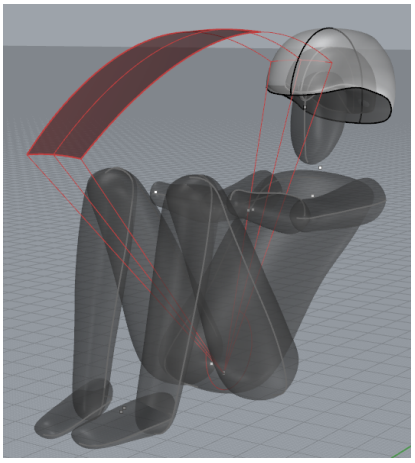

Figure 9: A 3D model of the driver and the occupant space

The suspension

The organization also had demands regarding turning circles and maneuverability:

2.20.1	Solar cars must be able to negotiate a Figure-8 course in less than 9 seconds per side and less than 18 seconds overall. (Two circles put together with a 6m radius)
2.20.2	Solar cars must be able to negotiate a slalom course in less than 11.5 seconds. (a 128m slalom with 18m in between each pylon)

These regulations, combined with building a suspension setup which could withstand all relevant load cases, resulted in a spatial budget which represented all possible wheel configurations, shown in Figure

10. These were then used to determine the space required for the wheel fairings, the height of the solar car and the three dimensional blend which connected the wheel fairings to the main body.

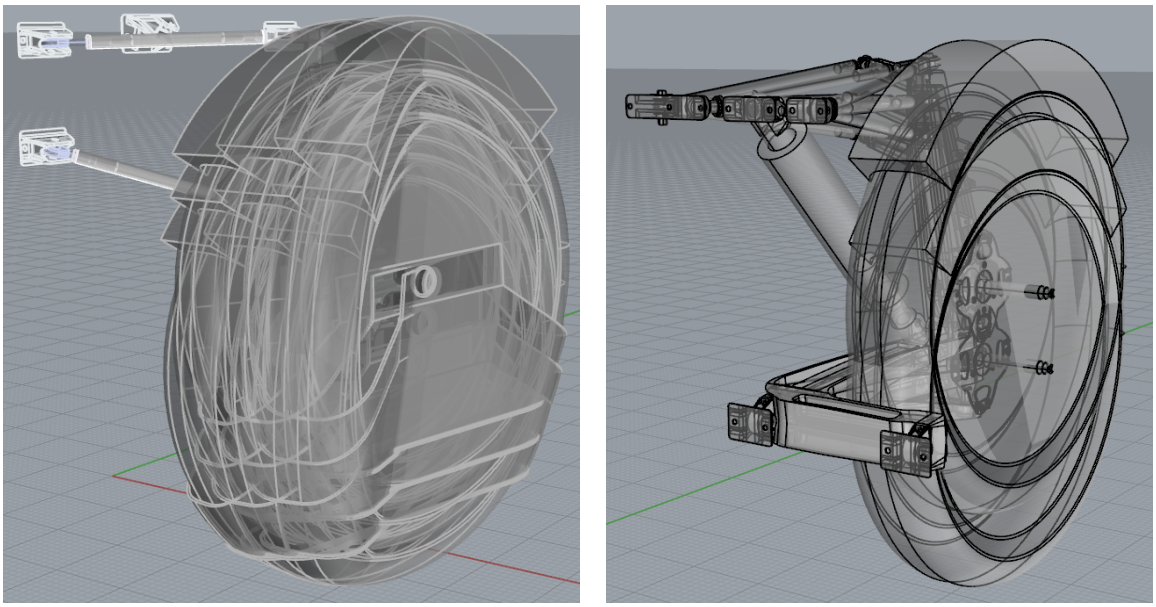

(a) All configurations for the front suspension.

(b) All configurations for the rear suspension.

Figure 10: The suspension configurations.

Solar cell array

One of the key components of the solar car is its solar cell array. There is a direct conflict between the interests of the electrical team and the aerodynamic team. The solar cell array is one of the key compromises in the solar car. A balance between energy generation of the solar cell array and minimizing aerodynamic drag must be achieved. In order to optimize this initially a solar cell model was used, which was programmed in Matlab and is shown in Figure 11.

Certain deficiencies in the model (i.e. not taking into account double curvature when placing the solar cells), led to modelling the solar cell placement in Rhinoceros 3D instead. This allowed for a more accurate three dimensional representation of the solar array, as shown in Figures 12a and 12b.

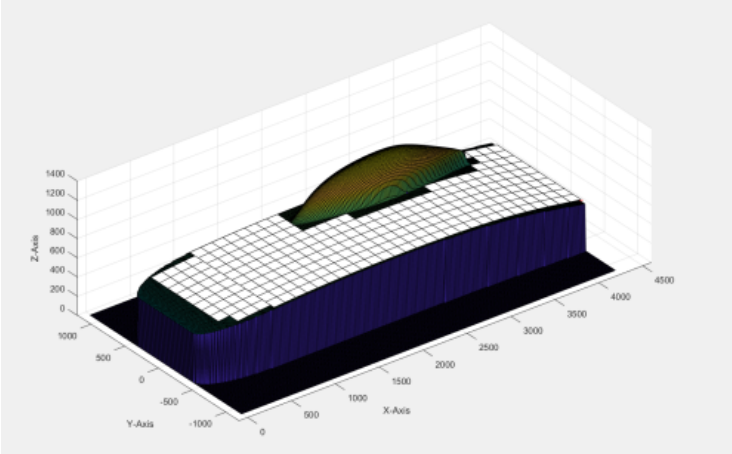

Figure 11: The solar array model used in the initial stages of the project

During the initial stages of the project, three different manufacturers were considered for the encapsulating laminate for the solar array. Each manufacturer used their own margins and spacing in between cells and sections, which meant that the recess had to be designed to fit three different array sizes, without

compromising the aerodynamic efficiency of the car. This was realized by projecting all different layouts onto the 3D model of the solar car and forming the recess around these layouts, shown in Figure 12.

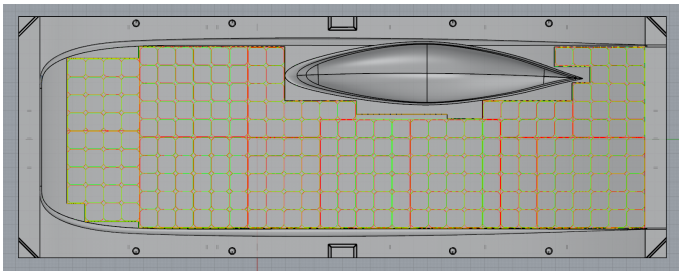

(a) A top view of the different array layouts

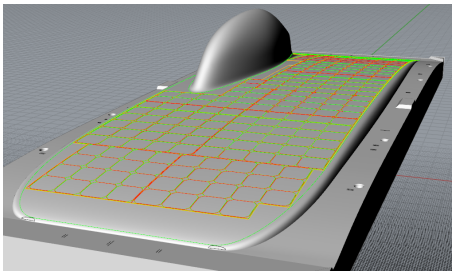

(b) A three dimensional view of the layouts

Figure 12: Modeling the recess as efficiently as possible.

4. Numerical model of the solar car

A numerical model was constructed in order to analyze the three dimensional airflow around the solar car. The numerical model was used to analyze the design choices made during the design process.

Mesh

The mesh of the solar car consists of multiple components. They are the surface mesh, inflation layer, near field mesh and far field mesh. The surface mesh, as the name implies, discretizes the continuous surface of the solar car. The inflation layer is then extruded normal to the surface from this surface mesh. After the extrusion of the inflation layer the immediate volume around the car is meshed with a volume mesh of relatively small size for greater accuracy, after which the far field is meshed with a larger mesh size to decrease the computational time necessary for the simulation. All meshes are unstructured.

The ANSYS [11] meshing module gives rather limited information and control regarding more detailed meshing options. It is therefore rather difficult to properly describe the mesh characteristics. The main advantage for the novice user is that it is quick and easy to automatically mesh new geometries with a relatively basic set of settings. The surface mesh is split into a fine and a coarse part.

The fine mesh is used for high curvature areas like the leading edges and wheel fairing blends. It uses a 3mm element size and curvature based size function with a maximum curvature normal angle of 18°. Mesh sizing is also adapted based on curvature and proximity (or in the case of surfaces, curvature only). The mesh elements are solely triangular, using a Delaunay algorithm. The coarse mesh size is similar, but uses a mesh size of 10mm.

The prediction of laminar-turbulent transition in the boundary layer is very important for an accurate shear drag estimate. To accurately simulate the boundary layer characteristics an inflation layer is built from the surface mesh. Initial layer thickness, max layers and growth rate are used to control the inflation layer. They are set to 5· 10^{-6} m, 35 and 1.3 respectively. The final y^+-value shown in Figure 13 for the simulations ranges from 0.01 to 0.50.

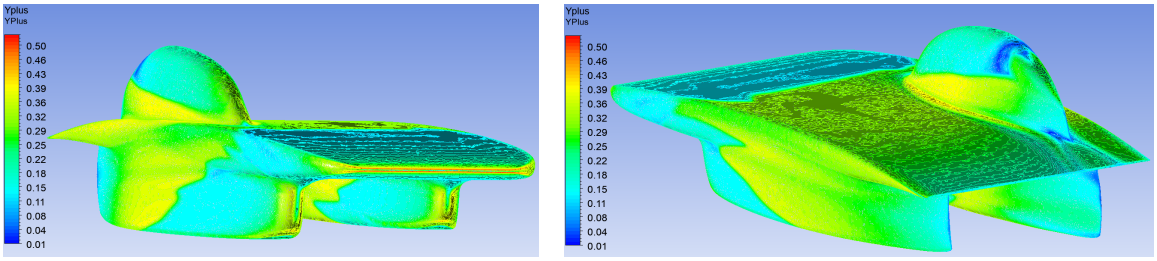

(a) The y^+ distribution at the front of the car.

(b) The y^+ distribution at the rear of the car.

Figure 13

The near field mesh volume element size is set to 40mm, with a proximity (neighbouring walls) and curvature based size function. The proximity min size is 1mm. The far field spacing is again very similar to the near field spacing, but the element size is set to 200mm. A cut of the mesh is shown in Figure 14a. The mesh consists of twenty million nodes and fifty million elements. Unfortunately ANSYS does not allow for a more detailed summary of the mesh elements.

CFD-pre setup

The simulation is set up using ANSYS CFX-Pre where a steady state simulation approach is selected. All simulations were run using an Air Ideal Gas model for the fluid, which in CFX-Pre means that the energy equation is also solved [12]. Since the simulation can be considered incompressible solving the

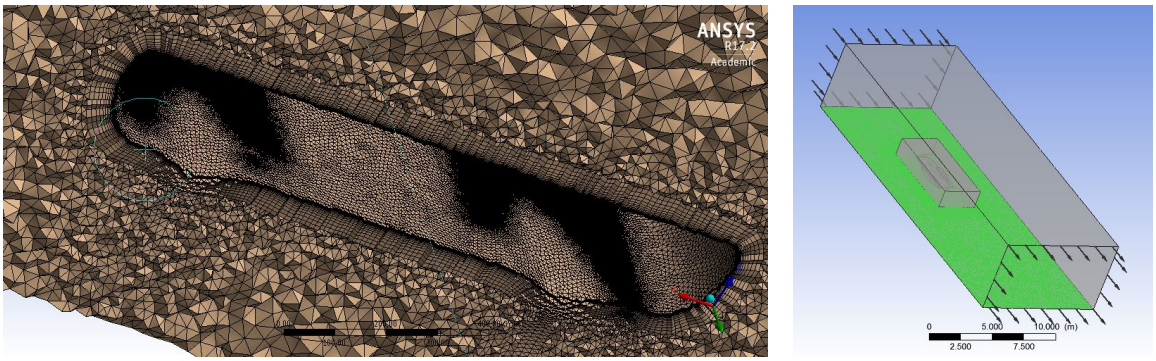

(a) A cut of the mesh.

(b) An illustration of the CFD sim.

Figure 14: The mesh and the CFD computational domain.

energy equation is not necessary and therefore it only slows down the calculations. The incompressible approach is something that must be looked into by the following team.

The model is considered to be isothermal, with a constant temperature of 35º C, which is the relevant temperature for Australia. The Shear Stress Transport model [13] is used to model turbulence, while the Gamma Theta model [14] is used to predict the transition in the boundary layer.

Both the body of the solar car and the ground are considered to be no-slip walls, with the ground having a velocity component of 22.84 m/s to simulate the movement of the solar car. The advantage of the velocity component on the ground is that a ground boundary layer is circumvented. The upstream inlet is considered as a velocity inlet with the same velocity as the ground. The outlet is a pressure boundary with an average static pressure of 1 atm (relative pressure 0 Pa). All other far field boundaries are treated as no slip walls with a velocity component of 22.84 m/s, which is the same as the flow velocity. A figure showing the car, nearfield and farfield is shown in Figure 14b.

Results analysis tools

All results were analyzed in ANSYS CFD-Post using a variety of analyses, which will be discussed in this section. It should be noted that the present section is not about the optimization of the solar car design, but focuses on the analysis techniques used to do so. The design of the solar car will be discussed at length in later sections of the report.

Wetted area A, drag area C_dA, shear drag $C_{d,s}$, pressure drag $C_{d,p}$

The wetted area is simply the total area which is exposed to the air flow, which determines the total shear drag of the solar car. The drag area (C_dA) can be calculated from the Reynold's drag equation:

$$F_d = \frac{1}{2}\rho C_d A V^2 \rightarrow C_dA = \frac{F_d}{\frac{1}{2}\rho V^2} \tag{1}$$

In the CFD simulation, the values for ρ and V are taken as a mass flow average over the inlet:

$$C_dA = \frac{F_{d_y}}{\frac{1}{2}\frac{\int \rho d\dot{m}}{\dot{m}}_{in}\left(\frac{\int V d\dot{m}}{\dot{m}}_{in}\right)^2} \tag{2}$$

Where F_{d_y} is the force in the y-direction due to pressure and shear drag. The shear drag in the y-direction is defined as:

$$\tau_y = \mu\frac{\partial^2 v}{\partial y^2} \tag{3}$$

From this the $C_{d,s}A$ is determined:

$$C_{d,s}A = \frac{\int \tau_y dA_{body}}{\frac{1}{2}\frac{\int \rho d\dot{m}}{\dot{m}}_{in}\left(\frac{\int V d\dot{m}}{\dot{m}}_{in}\right)^2} \tag{4}$$

The $C_{d,p}A$ is calculated in a similar fashion:

$$C_{d,p}A = \frac{\int p\boldsymbol{n}_y dA_{body}}{\frac{1}{2}\frac{\int \rho d\dot{m}}{\dot{m}}_{in}\left(\frac{\int V d\dot{m}}{\dot{m}}_{in}\right)^2} \tag{5}$$

Planar C_p plots

The coefficient of pressure is a parameter for studying the flow of incompressible fluids:

$$C_p = \frac{p - p_\infty}{p_0 - p_\infty} = \frac{p - p_\infty}{q_\infty} \tag{6}$$

Where:

- p is the static pressure at the evaluated point
- p_∞ is the static pressure in the freestream flow
- p_0 is the stagnation pressure in the freestream flow
- q_∞ is the dynamic pressure in the freestream flow

The planar plots were used to analyze the 2D C_p distribution across the surface of the solar car for certain slices in the 3D space. They were mostly used to analyze 3D effects on the 2D airfoil designs used for the solar car. The canopy was initially designed as a symmetrical airfoil which conformed to all demands mentioned in Section 2.2, while minimizing shear and pressure drag (more on this in later sections).

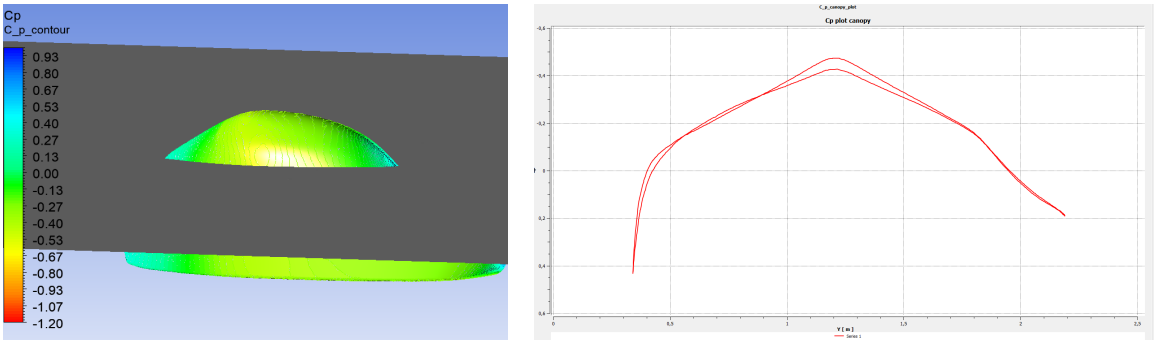

(a) The C_p plane shown in 3D space

(b) The C_p plot.

Figure 15: The 2D planar C_p approach for the canopy

From earlier editions (and basic aerodynamic understanding) it was known that 3D effects would play an important role in the fluid flow around the canopy. The canopy is located on the right side of the solar car. The choice is made because the race is driven north to south, which means that the sun will be left of the car for the majority of the day. Placing the canopy on the left side would cast a shadow on the solar array during the entire day.

The flow on the right side of the canopy the flow is unobstructed, while on the left of the canopy this is not the case. The boundary layer flow of the main airfoil (on which the solar array is located) interferes with the left side canopy boundary layer, while on the right side of the canopy this does not happen. The flow interaction results in a difference in flow velocity between the left and right side of the canopy,

which in turn results in a pressure differential. Flow separation did not occur in the 2D design, because it does not take 3D effects into account. In the 3D scenario flow separation does occur due to interference effects on the left side because due to the lower flow velocity on the left side of the canopy the adverse pressure gradient can no longer be overcome.

The C_p plot over the surface of the canopy shown in Figure 15 allowed us to analyze the induced camber on the canopy and allowed us to introduce the right amount of opposite geometrical camber to the canopy to cancel out the negative effects.

The planar C_p plots were also used for the design of certain aspects of the wheel fairings and the main airfoil, which will be discussed in Section 5.

C_p contour

Similar to the planar C_p plots, a contour plot over the surface was generated which showed the iso-pressure lines over the surface. The C_p contour was used to analyze the stagnation of the airflow at the leading edges of the wheel fairings and its influence on the flow surrounding them. The stagnation at the leading edges of the wheel fairings creates a pressure region around the wheel fairings which must be accounted for.

By shaping the fillets from the main airfoil to the wheel fairings the pressure distribution surrounding the leading edges could be influenced. Without the fillets the C_p gradient was very large, causing the boundary layer flow to quickly deflect into the main airfoil flow. This caused transition to occur much earlier than intended. By shaping the fillets the pressure gradient could be made much more gradual, deflecting the boundary layer flow as late as possible. This effect was analyzed using the C_p surface contour shown in Figure 16.

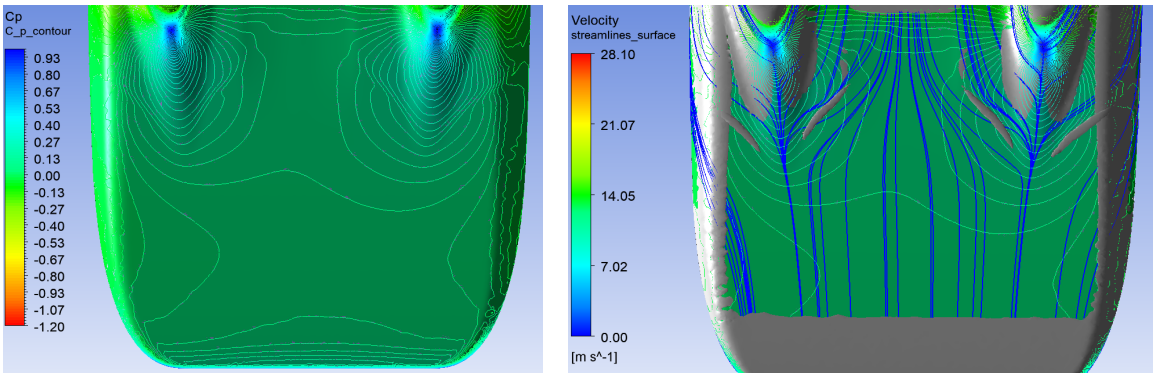

(a) The C_p contour over the surface near the leading edges of the wheel fairings

(b) Flow pattern around the wheel fairing leading edges

Figure 16: The flow situation surrounding the wheel fairing leading edges

Turbulence kinetic energy

The Turbulence Kinetic Energy was used during the later stages of the design phase to predict the transition from laminar to turbulent flow. Turbulence Kinetic Energy is the mean kinetic energy per unit mass associated with eddies in turbulent flow [15].

The Shear Stress Transport model is a k-ω-model which is based on the Reynolds Averaged Navier Stokes (RANS) equations [16]. For RANS, the turbulence kinetic energy can be quantified by the mean of the turbulence normal stresses:

$$k = \frac{1}{2}\left(\overline{(u')^2} + \overline{(v')^2} + \overline{(w')^2}\right) \tag{7}$$

k-ω models also use the Boussinesq approximation [17], which assumes isotropy of turbulence. Because of this isotropy assumption the turbulence kinetic energy kan be simplified even further:

$$k = \frac{3}{2}\overline{(u')^2} \tag{8}$$

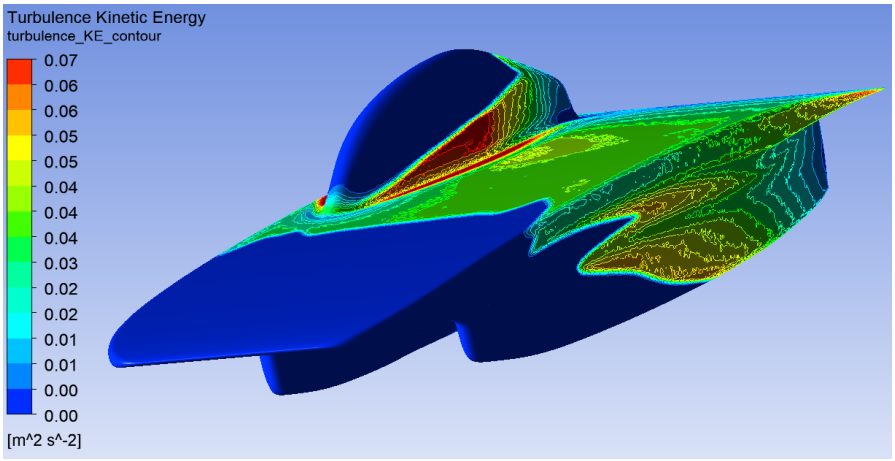

Figure 17: The turbulence kinetic energy distribution over the surface.

When this turbulence kinetic energy is subsequently plotted on the body of the solar car as in Figure 17, it provides a good impression of the turbulence present in the boundary layer. This knowledge was used for the optimization of the fillets and in doing so delay the transition in the boundary layer for as long as possible.

Total pressure losses

The evaluation of predicted total pressure losses was also a contribution by Hans. Assuming isentropic flow of a calorically perfect gas and also assuming that the flow is adiabatic, any change in the total pressure in the fluid domain will be caused by the rotation (i.e. turbulence) of the flow. The ratio of the total pressure to the absolute pressure can be written as:

$$\frac{P_T}{P_A} = \left(1 + \frac{\gamma - 1}{2} \cdot M^2\right)^{\frac{\gamma}{\gamma - 1}} \tag{9}$$

Where:

M is the Mach number
γ is the heat capacity ratio

If this is then multiplied by the absolute pressure P_A the total pressure at that point in the flow field can be calculated. This value is then compared to the area averaged total pressure at the inlet of the flow field:

$$P_{T_{in}} = \frac{\int P_A dA}{A}_{in} \left(1 + \frac{\gamma - 1}{2} \cdot \left(\frac{\int M dA}{A}_{in}\right)^2\right)^{\frac{\gamma}{\gamma - 1}} \tag{10}$$

From which the ratio between the total pressure at the inlet and any point in the flow field can be calculated. The *total pressure loss* is then defined as [18]:

$$TPL = 1 - \frac{P_A \left(1 + \frac{\gamma - 1}{2} \cdot M^2\right)^{\frac{\gamma}{\gamma - 1}}}{\frac{\int P_A dA}{A}_{in} \left(1 + \frac{\gamma - 1}{2} \cdot \left(\frac{\int M dA}{A}_{in}\right)^2\right)^{\frac{\gamma}{\gamma - 1}}} \tag{11}$$

The total pressure losses were used to analyze the vortices behind the solar car as shown in 18, like the vortices shed by the canopy and wheel fairings.

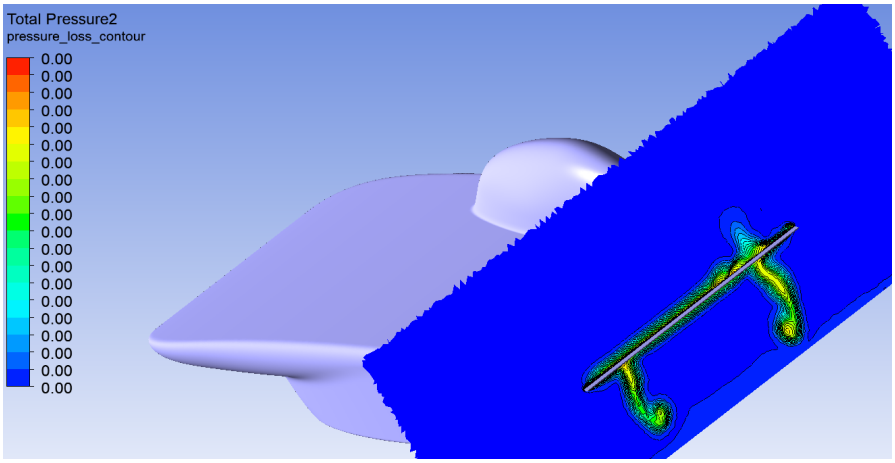

Figure 18: The total pressure losses plotted on a plane behind the solar car.

5. Theoretical design of RED Shift

The first design

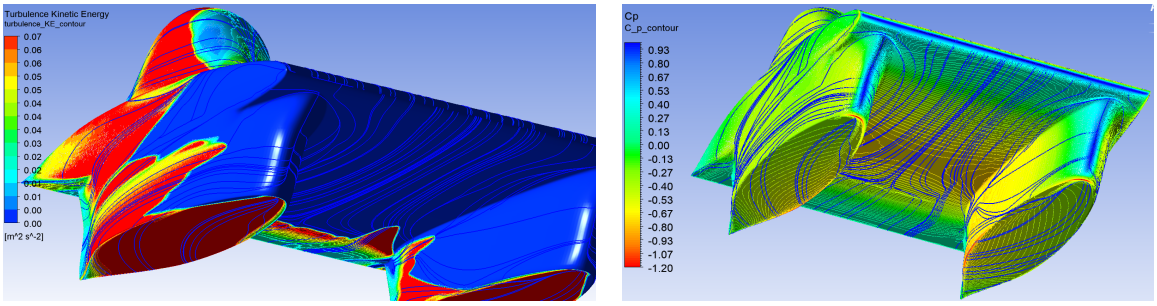

(a) The TKE of the first design

(b) The cp/streamlines plot for the first design

Figure 19: The very first design for the solar car.

The initial design shown in Figure 19 is provided here as a point of reference or a baseline design. At this point in the project it was quite a challenge to design a car, let alone design it aerodynamically. The initial configuration does demonstrate the basic approach to designing RED Shift fairly well though. As a basis, 2D airfoils are used which are extruded and blended together to form what is essentially already a catamaran solar car. For this design, the 2015 canopy was used which needed a complete redesign. However, both the main airfoil and the wheel fairings were 6-series airfoils (NACA 67007 & NACA 67015 respectively). The track width and wheel base were still set to 1300mm and 2100mm respectively, as advised by the 2015 team. The C_dA value of 0.0994 m^2 for this first design would eventually almost be beaten by the practical value for the real car, including wheels, solar array, separating seems etc.

It is impossible to discuss every single iteration, so the most relevant milestones will be discussed instead. Any changes made in between these milestones will be covered.

Main airfoil design

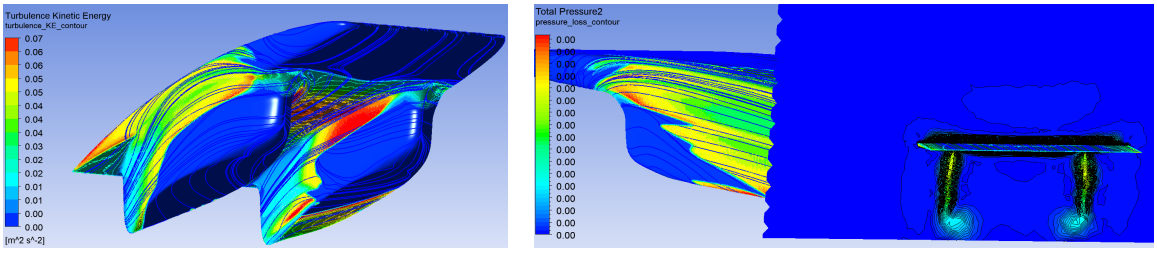

(a) The laminar BL flow is now preserved beyond the leading edge of the solar car

(b) Vortex shedding is observed near the bottom of the wheel fairings

Figure 20: Big steps forward have been made by iteration 8.

During the first few iterations the design considerations mentioned in Sections 3.2 and 3.3 were applied. The wheel fairings were also moved backwards, to increase the area over which the laminar boundary layer flow would not be interfered with by the wheel fairing leading edges. Cambered wheel fairing airfoils were introduced to compensate for the venturi effect in between the wheel fairings. The first lift producing main airfoil were also introduced to further compensate for the venturi effect. The blends between the main airfoil and the wheel fairings were improved, as were the bottom wheel fairing fillets.

The canopy was omitted during this stage of the body design. This choice was made because it saved on computational time, but also because no representative canopy was available at this time. The design of the canopy was performed in parallel to the development of the main body of the solar car.

A size estimate was made to determine the dimensions of the main airfoil which was needed to fit the 4m^2 solar array, as already illustrated by Figure 11. This estimate initiated the 3D shape of the leading edge of the solar car into a more aerodynamic shape as can be seen in Figure 20. The front corners of the main airfoil were rounded to prevent immediate flow separation while still allowing the placement of the solar array. The sides of the car were swept using one continuous shape which only varied in the z-direction (height).

Eventually the placement estimate of the array would turn out to be wrong, as the model only accounted for uni-directional curvature and did not take double curvature limits into account. At this point the total width of the solar car was already set, but the problem was overcome by decreasing the upper radius of the main airfoil side sweep to increase the single-curved surface area on the top of the array. This fortunately only took one iteration to fix.

Left wheel fairing ground clearance

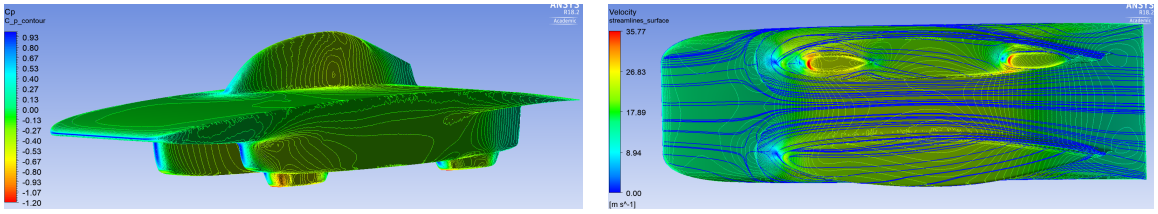

(a) The C_p distribution for the 120mm case.

(b) The surfaces streamlines show that the flow is sucked into the low pressure volume underneath the car.

Figure 21: The analysis of the 120mm ground clearance, including wheel casings

As more and more of the mechanical and structural design demands were set in stone, the aerodynamics team was left with decreasing options to reduce the effects of the venturi under the car. Increasing maneuverability demands set by the organization and a call made by the electrical department that the overly complicated rear wheel steering system would not return for this car resulted in large lateral front wheel displacements. Increased safety demands set by the organization saw an increase in occupant cell (the area surrounding the driver) size. The presence of various electrical system and structural support ribs further limited the design freedom for the aerodynamics department. All the while, the downforce generated by the venturi kept increasing beyond expected levels with each design iteration.

The downforce increase resulted in the eventual call to look into increasing the ground clearance of the wheel fairings to reduce the adverse effects of the venturi and with it reduce the large amount of downforce. The driver's wheel fairing was quickly ruled out, as increasing its ground clearance would also increase the head height of the driver and therefore complicate the canopy design. Three new designs were made with various ground clearances for the left wheel fairing. 60mm, 80mm, 100mm and 120mm with wheel casings present ground clearance was analyzed for the left wheel fairing as shown in Figure 21.

The effect of rotating wheels was omitted because the amount of exposed wheels was the same in all situations. Because any exposed wheel beyond the minimum ground clearance of 60mm was covered by the casings. At 120mm ground clearance the extra pressure drag created by the exposed wheel casings turned out to be less than the induced drag caused by the low pressure region under the car

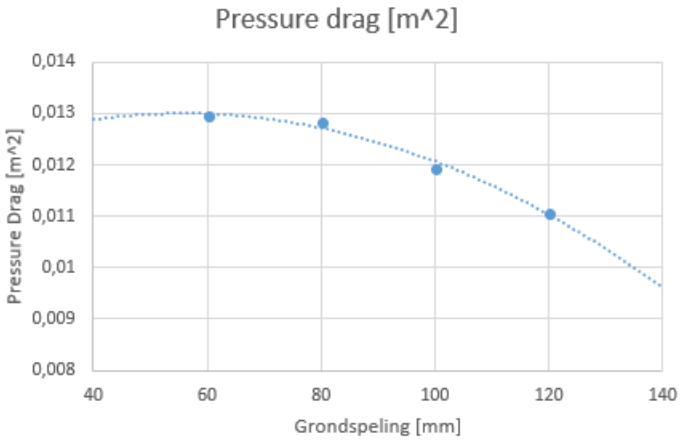

Figure 22: The pressure drag reduces with increasing ground clearance.

and the shear drag caused by the extra surface area of the original design. The variation in pressure drag for increasing left wheel fairing ground clearance is plotted in Figure 22.

Canopy design

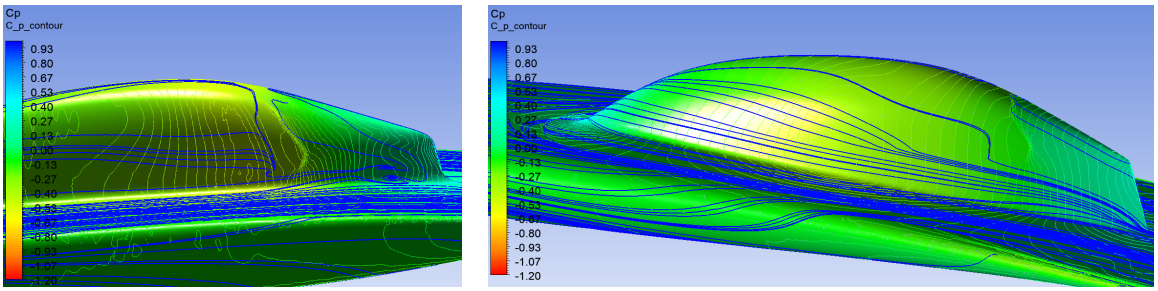

(a) Initial 6-series canopies all suffered from flow separation because of a steep adverse pressure gradient

(b) Moving away from the 6-series profile the adverse pressure gradient was eventually dealt with.

Figure 23: The canopy design slowly turned into a completely custom design

For the 2017 competitor, a complete redesign of the canopy was necessary, of which the design is shown in Figure 23. A proper redesign of the canopy was not undertaken since the 2013 edition of the solar team and with a completely new CAD modeling program designing a new canopy from scratch was a big challenge. Initially the main concern was creating a design which could fit the driver, the rollbar and the occupant space demands set by the organization. It quickly became apparent that fitting everything inside the canopy while preventing flow separation would result in a massive canopy and the 6-series profile was quickly replaced with a mostly custom design.

To reduce surface area, a test was performed where the rear half of the canopy was chopped off as shown in Figure 24. The recirculation volume behind the chopped of canopy was then used as an estimate to create an updated design with a tail that only just filled up this volume, removing a large chunk of functionless surface area. A loophole in the regulations regarding the occupant space demands (shown in Figure 9) was found. Its placement inside the occupant cell was defined by the position of the back support of the seat. By moving the bottom part of the seat back rearward this occupant space demand was positioned in a much more convenient place, significantly reducing the length of the canopy and with it the wetted area.

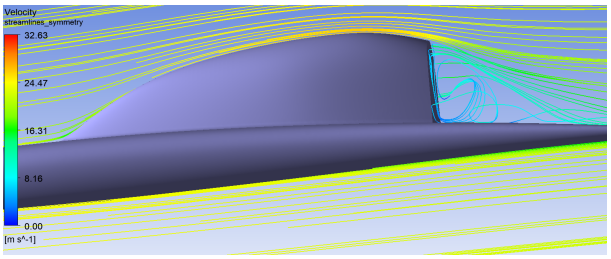

(a) The canopy was cut after its widest point to estimate the necessary tail size

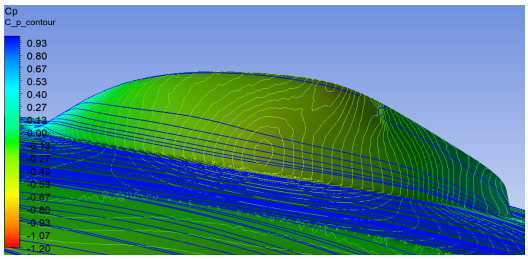

(b) The final canopy was then formed using the CFD results of the cut canopy, camber was also added.

Figure 24: The canopy design approach

The canopy was initially designed for a central position on the car to obtain a good first estimate of the correct shape. Once it was moved to the designated position on the right side an asymmetric pressure distribution, as discussed previously in Section 4.3.2, was observed. This was expected and it was quickly fixed by slightly cambering the 3D design of the canopy to compensate for this effect. Its presence on the car did have a larger than expected effect on the trailing edge of the driver's wheel fairing, which would subsequently be tackled.

Wheel fairings twist & variable fillets

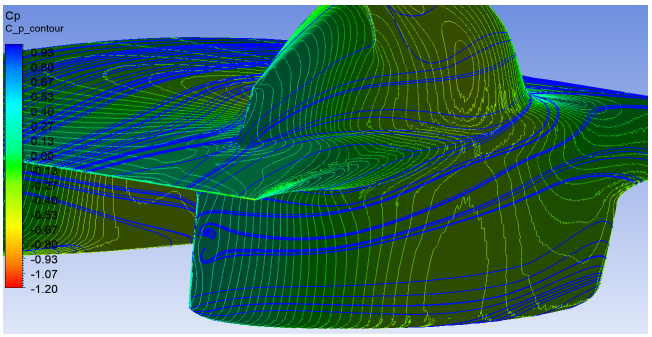

(a) The presence of the canopy resulted in a small recirculation area at the trailing edge of the driver's wheel fairing

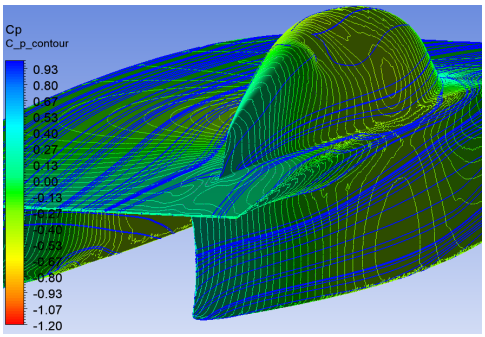

(b) Adding a slight twist to the driver's wheel fairing solved the problem

Figure 25: Adding a twist to the trailing edge of the wheel fairing to prevent a recirculation area from forming

The presence of the canopy on the right side of the solar car changed the C_p distribution on the driver's wheel fairing as shown in Figure 25. This was expected, however it affected the region near the trailing edge of the driver's wheel fairing more than was initially expected. The boundary layer flow was no longer able to overcome the adverse pressure gradient present there and the flow separated. This was solved by locally adding twist to the wheel fairing, since by this stage far reaching changes to the wheel fairing's airfoil base shape was no longer possible.

Air flowing under the wheel fairings was also sucked into the tunnel under the car because of the low pressure region created by the increased flow velocity. The flow that separated from the bottom of the wheel fairings into the tunnel rolled of the small inside radii creating vortices in the flow that could clearly be seen in the pressure loss plane behind the solar car. Increasing the fillet radius where this was possible decreased the vorticity present in the downstream flow as shown in Figure 26.

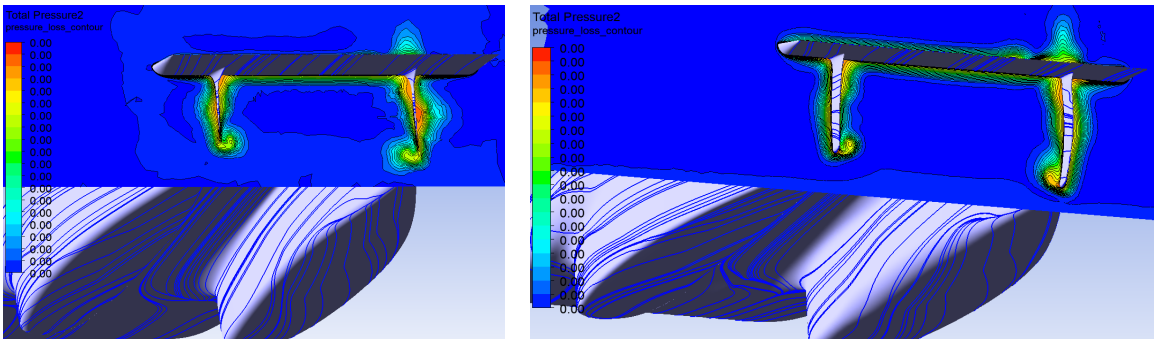

(a) The pressure loss planes clearly shows the vortices present on the inside of the wheel fairings

(b) This effect was subsequently reduced by increasing the fillet radius where possible.

Figure 26: The pressure loss plane allowed the analysis of the vorticity of the flow behind the solar car.

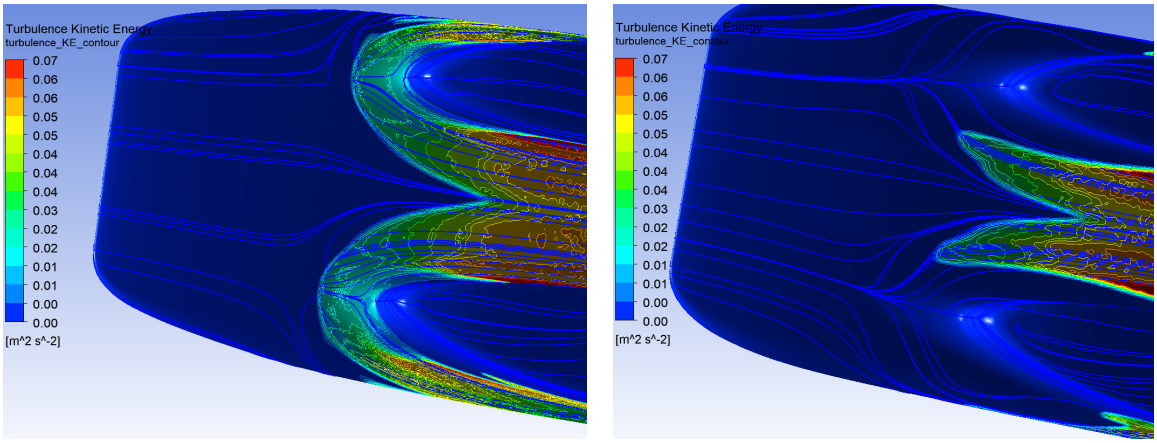

(a) Without proper fillets the flow trips almost immediately, greatly increasing shear drag.

(b) With fillets, the tripping of the flow is delayed as long as possible.

Figure 27: The design of the fillets greatly reduced the shear drag of the solar car.

Fillets

The presence of the wheel fairings had a big influence on the airflow under the solar car. The associated leading edges created additional stagnation regions in the airflow downstream of the main leading edge of the solar car. This created pressure regions in front of these leading edges as shown in Figure 16. Initially there was little to no fillet present in front of the wheel fairing leading edges. The boundary layer flow which approached the leading edges had to deal with a very large adverse pressure gradient, which caused the flow to trip to turbulent BL flow. This of course increased the shear drag component by a significant amount.

The curvature from the main airfoil to the wheel fairings was made more gradual and the right curvature development was judged based on the C_p distribution leading up to the wheel fairing leading edges. Too fast an increase in pressure was avoided for as long as possible, greatly reducing the tendency for the boundary layer flow to trip and become turbulent as illustrated in Figure 27.

The following drag values are associated with the design shown in Figure 27a: C_dA: 0.0614, $C_{d,p}A$: 0.0175, $C_{d,s}A$ 0.0441. The following drag values are associated with the design shown in Figure 27b: C_dA: 0.0555, $C_{d,p}A$: 0.0137, $C_{d,s}$: 0.0415.

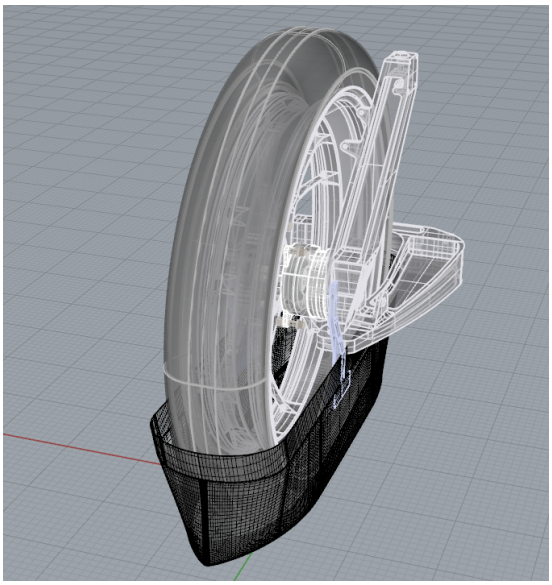

(a) The wheel casings were modeled to fit around the tires and attach to the hubs.

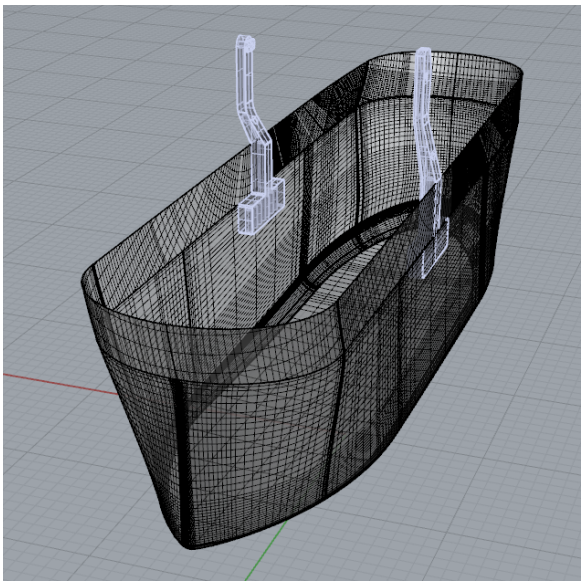

(b) The wheel casing design without the tire.

Figure 28: Wheel casing design.

Wheel casings

I was not too much involved in designing the wheel casings, as I was mostly focused on the banked road tests in this project phase. But for completeness I will give a short description. The rotating wheels are one of the biggest sources of aerodynamic drag on the solar car. One of our concerns during the design of RED Shift was to minimize the pressure drag created by the tires. Three solution were thought of. The first solution was to cover as much as possible of the rotating wheel with the wheel casings as shown in Figures 4 and 29. Their effectiveness in reducing the pressure drag was already proven by the 2015 team in the windtunnel, and it was our job to improve them. The biggest improvement here was their connection to the hub of the wheels.

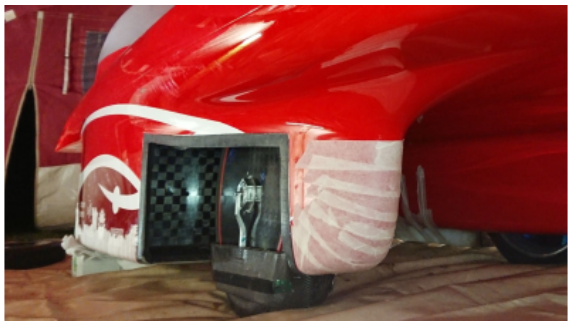

(a) The wheel casings as eventually fitted on the car.

(b) The covers that were used to seal up the wheel arch openings.

Figure 29: Strategies used to reduce the pressure drag cause by the exposed wheels.

The second part of the solution was to coverthe openings around the tires with a latex membrane to prevent airflow into the wheel arches. The last measure to reduce the pressure drag created by the tires was the use of splitters, which will be discussed in the windtunnel section. One of the future goals is to test setups like this in the windtunnel, with a rolling road, rolling tires etc.

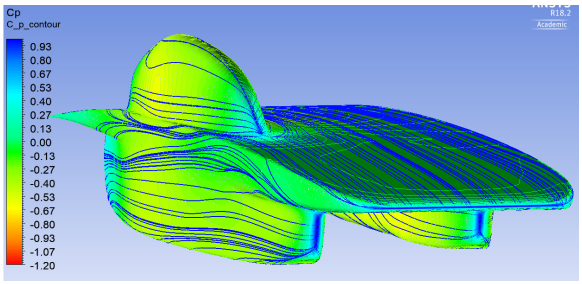

(a) The streamlines/C_p plot for the final design.

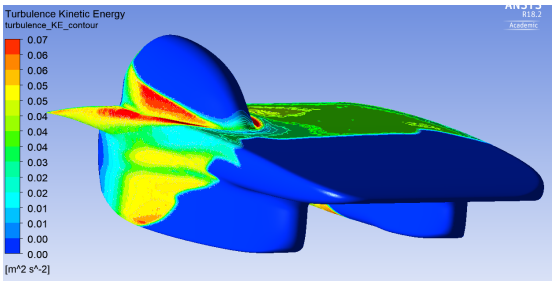

(b) The turbulence kinetic energy for the final design

Figure 30: The final design, seen from the front

The final design

The final design for RED Shift incorporates all the design choices mentioned earlier in this Section. The track width and wheel base were changed while the ground clearance for the left wheel hub was increased to mitigate the effects of the venturi. The wheel fairings were moved backwards, while the main airfoil design was improved and an entirely new canopy design was implemented. The fillets for the canopy and wheel fairings were optimized to delay the laminar-turbulent transition as much as possible, reducing drag. Completely custom airfoil designs were used for each aspect of the car, and 3D aerodynamic design like the variable fillets and the twist to the wheel fairings was used to further optimize the design. Some of the results are plotted in Figures 30, 31 and32, while the drag numbers are listed in Table 4.

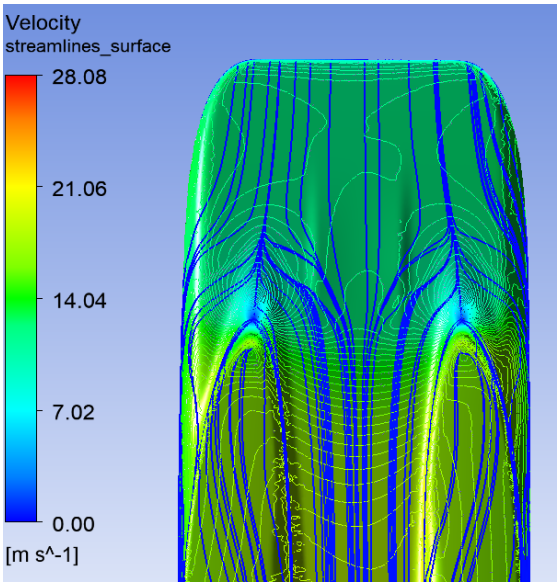

(a) The streamlines/C_p plot for the final design.

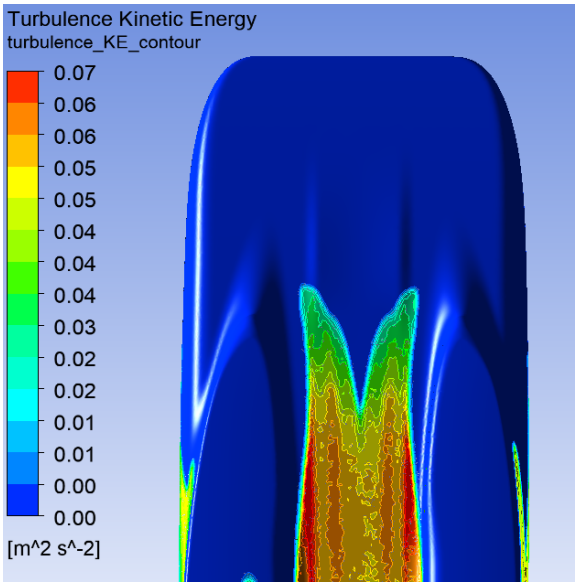

(b) The turbulence kinetic energy for the final design

Figure 31: The final design, seen from the bottom

Table 4: The results for the final design of the solar car

Wetted Area (m^2)	C_dA **(m^2)**	$C_{d,p}A$ **(m^2)**	$C_{d,s}A$ **(m^2)**	**Downforce (N)**
17.04	0.0555	0.0137	0.0415	79.6

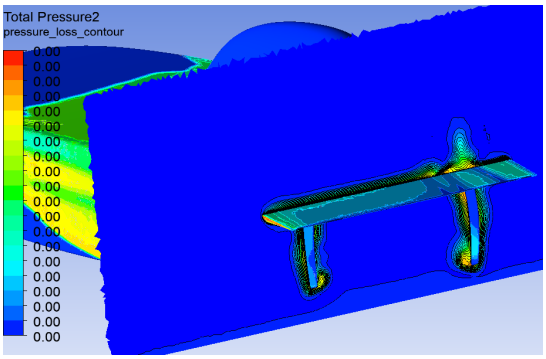

(a) The total pressure losses plotted right behind the canopy.

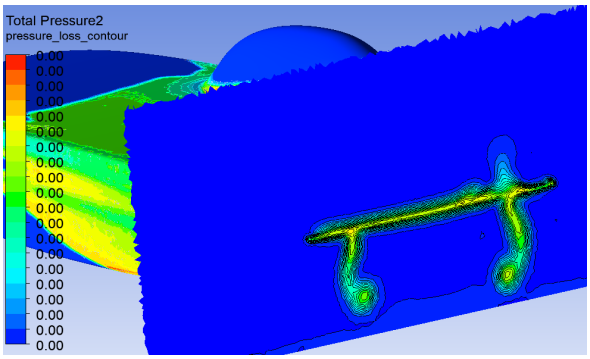

(b) The total pressure losses plotted right behind the solar car

Figure 32: The final design's total pressure losses

6. Windtunnel

In July one weekend was spent at the windtunnel of DNW to test various aspects of the solar car. Some of these tests would validate the results found by the theoretical CFD model. Other aspects could not be tested using CFD and would therefore be conducted in the windtunnel. In the previous editions only scale model tests would be possible, due to the size of the windtunnel. With the new regulations, however, the entire car could finally fit into the windtunnel which allowed for full scale tests to take place.

The physical setup

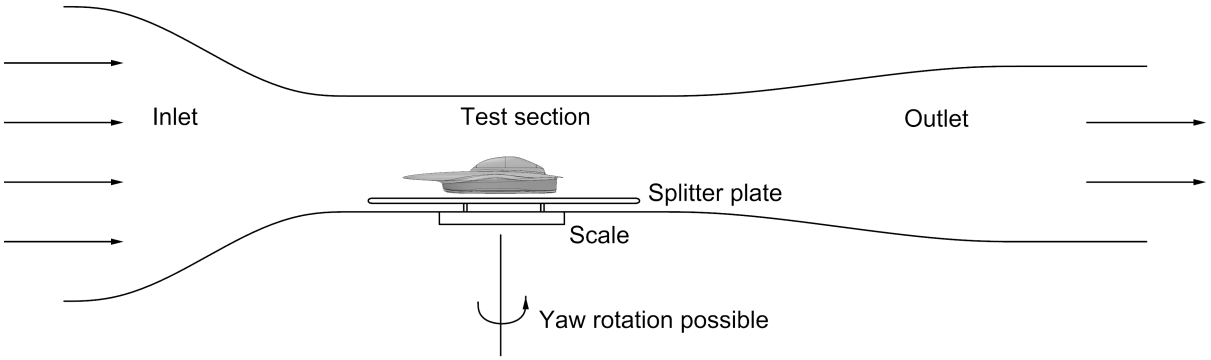

Figure 33: The general layout of the windtunnel (simplified)

The solar car was mounted on a large splitter plate as shown in Figure 33. This removed the floor boundary layer and simulated the road conditions as best as possible, since a rolling road setup was not possible in the DNW windtunnel. This splitter plate was in turn mounted on the windtunnel's balance, which measured all aerodynamic forces on the solar car. The measurement accuracy of the balance was 0.25-0.5 N, as reported to us by DNW. Some comparative tests yielded a difference in results smaller than this and were therefore inconclusive. The alpha sweep (pitch angle), discussed in Section 6.4.3, is a good example of this.

The test plan

The initial testplan is listed in Table 5. Due to time constraints during the actual windtunnel testing, not all of these subtests could be performed. Most tests were reduced to larger intervals. For example, the alpha sweep test (pitch angle) would still be performed, but with larger intervals in front and rear damper height to save time. The general trend of all tests could still be observed with these larger intervals, so no information was lost.

Because of its size, Table 5 is listed on its own page.

Table 5: The initial test plan for the windtunnel tests (LE = Leading Edge).

Zero Measurement	**Velocity (km/h)**	**Yaw angle (°)**	**Roll angle (°)**
	70	[-6, -4, -2, 0, 2, 4, 6]	0
	85	[-6, -4, -2, 0, 2, 4, 6]	0
	100	[-6, -4, -2, 0, 2, 4, 6]	0
Trips strips	**Velocity**	**Trip strip location**	
	70	Top main airfoil	
	85	Top main airfoil	
	100	Top main airfoil	
	75	Bottom main airfoil	
	85	Bottom main airfoil	
	100	Bottom main airfoil	
	70	LE right wheel fairing	
	85	LE right wheel fairing	
	100	LE right wheel fairing	
	70	LE left wheel fairing	
	85	LE left wheel fairing	
	100	LE left wheel fairing	
Roll Angle	**Velocity (km/h)**	**Yaw angle (°)**	**Roll angle (°)**
	70	[-6, -4, -2, 0, 2, 4, 6]	[-1.4, 1.4]
	85	[-6, -4, -2, 0, 2, 4, 6]	[-1.4, 1.4]
	100	[-6, -4, -2, 0, 2, 4, 6]	[-1.4, 1.4]
Angle of Attack	**Velocity (km/h)**	**Front damper height (mm)**	**Rear Damper height (mm)**
	85	5	0
	85	10	0
	85	15	0
	85	20	0
	85	0	5
	85	0	10
	85	0	15
	85	0	20
Splitters	**Velocity km/h)**	**Concept variant**	**Steering angle (°)**
	85	No Splitters	[-5, 0, 5]
	85	Concept A	[-5, 0, 5]
	85	Concept B	[-5, 0, 5]
Smoke visualization	**Velocity (km/h)**	**Yaw angle (°)**	
	70	[-6, -4, -2, 0, 2, 4, 6]	
	80	[-6, -4, -2, 0, 2, 4, 6]	
	100	[-6, -4, -2, 0, 2, 4, 6]	

The results

During all tests the forces on the car were measured continuously by the balance to which the car was mounted. These forces could subsequently be converted into the C_dA of the car using the drag coefficient equation:

$$F_D = \frac{1}{2}\rho v^2 C_d A \tag{12}$$

All figures in this section have *dragcount* C_dA $(10^{-4}m^2)$ plotted on the y-axis and the various yaw angles on the x-axis. The specific measurement is listed in the graph's title.

Zero Measurement

An initial zero measurement was conducted to arrive at a reference for all future tests. By doing this all other tests which deviated from the standard configuration could be compared to a control configuration to measure their respective performance. A zero measurement was conducted for just the splitter plate with no car mounted on top (Figure 34). Another zero measurement was performed with the car in its control configuration (Figure 35).

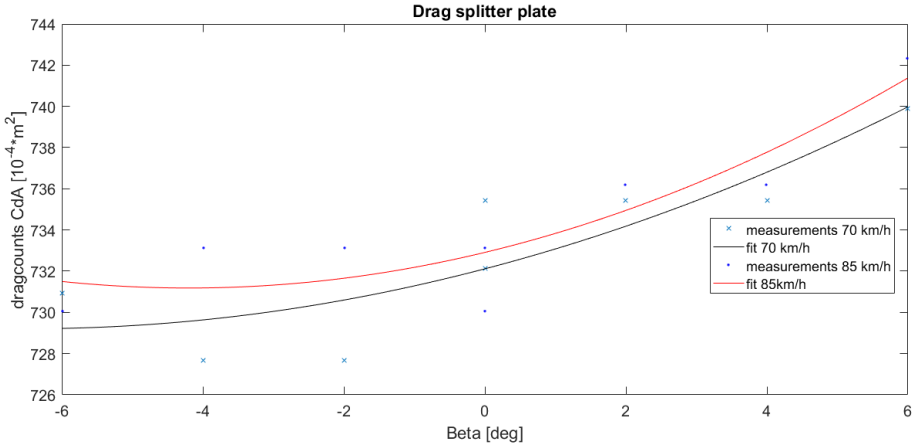

Figure 34: One dragcount C_dA is equal to approximately 0.2 N.

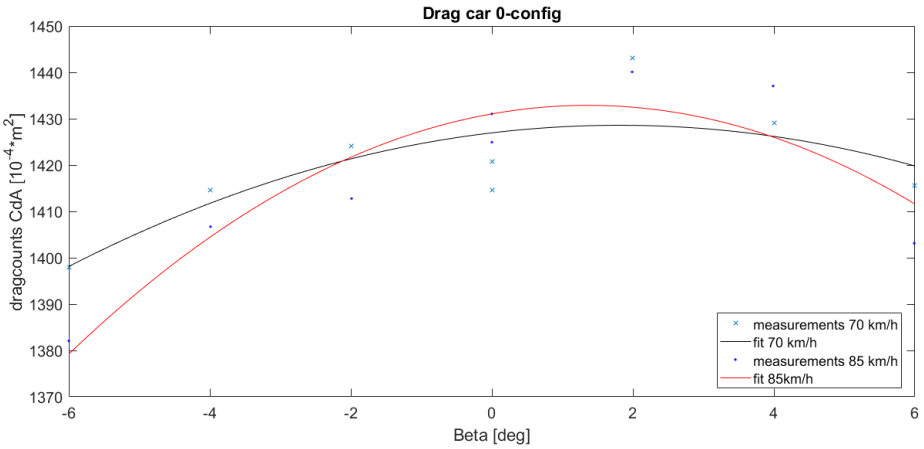

Figure 35: The zero measurement performed with just the splitter plate and the car present

One interesting observation, albeit expected, is that the drag of the solar car decreases for increasing yaw angles. This happens because the wheel fairings of the catamaran start to function similar to boat sails [19] with sidewind. The deflection of the sidewind on the wheel fairings results in a suction force

in the direction of travel, resulting in a reduction of the overall drag. This result is in agreement with previous CFD analyses performed for sidewind conditions.

Trip strips

Initially, the plan was to apply trip strips to many places on the car in order to investigate the presence of laminar flow regions on those parts of the car. Unfortunately we were only given two days of measurements to do all the tests, so a number of these sub tests had to be scrapped. The tests that remained were:

- Trip strips on the bottom of the nose
- Trip strips on the top of the nose
- Fully turbulent measurement (all leading edges)

These tests were intended to verify the presence of laminar boundary layer flow over the top and bottom of the solar car as well as the downstream leading edges.

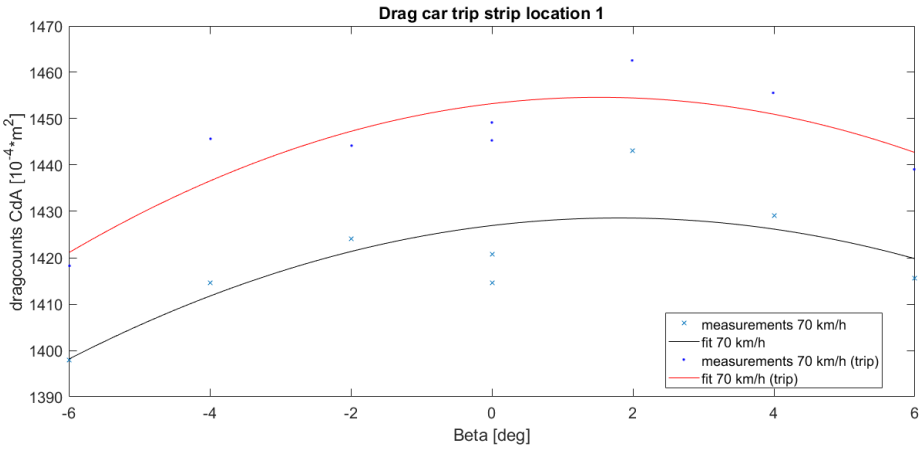

Figure 36: The difference in C_dA due to the trip strip located on the bottom of the main airfoil leading edge, right behind the leading edge.

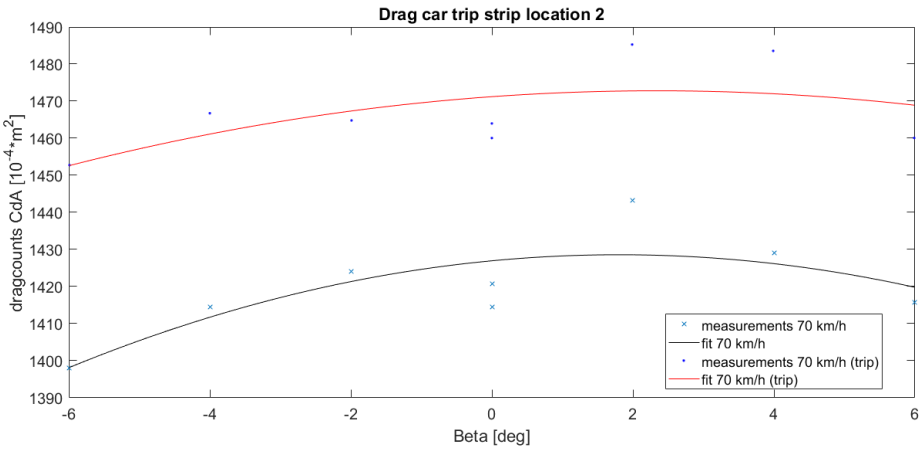

Figure 37: The difference in C_dA due to the trip strip located on the top of the main airfoil leading edge, right behind the leading edge.

The measurement results show a significant difference for the tests without trip strips and the test with trip strips (Figure 36, 37, 38). Therefore, evidence was found that a significant amount of laminar flow was not only present on the bottom of the main airfoil, but also on the top of the main airfoil as well as after any downstream leading edges. These tests were also performed at a higher speed of 85 km/h and the measurement results are very similar.

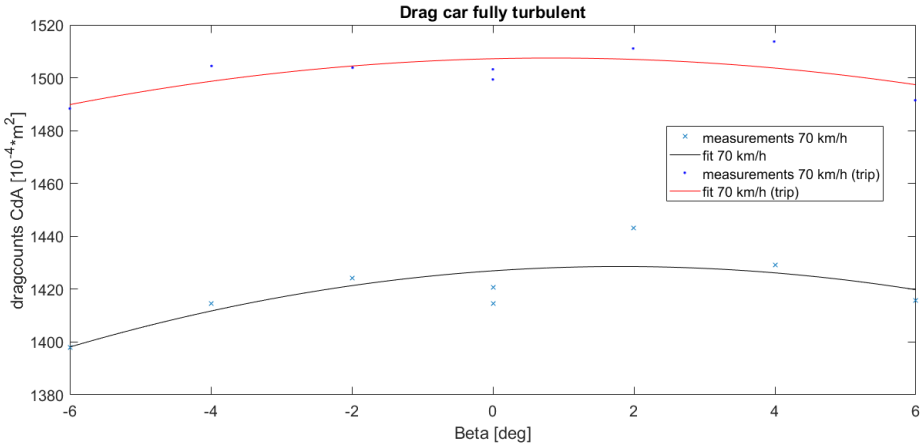

Figure 38: The difference in C_dA for a fully turbulent analysis of the solar car.

Roll analysis (variable ride height)

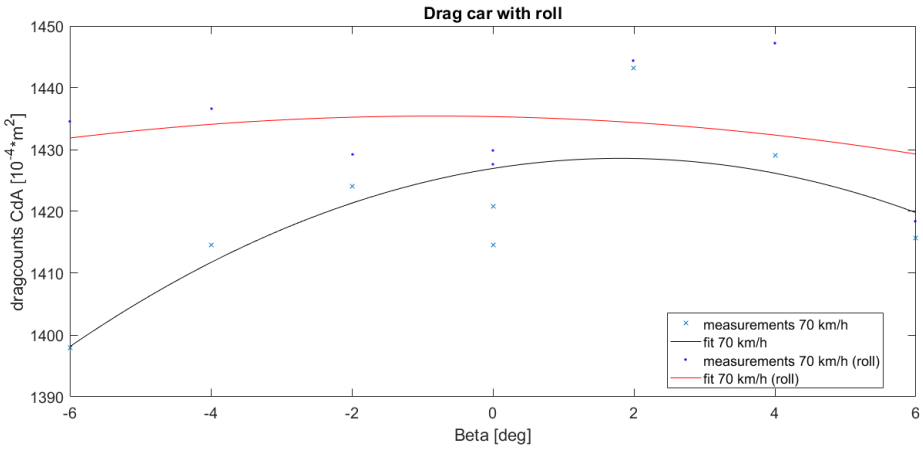

Figure 39: The dragcount comparison between no roll and 1.4º of roll angle at 70 km/h

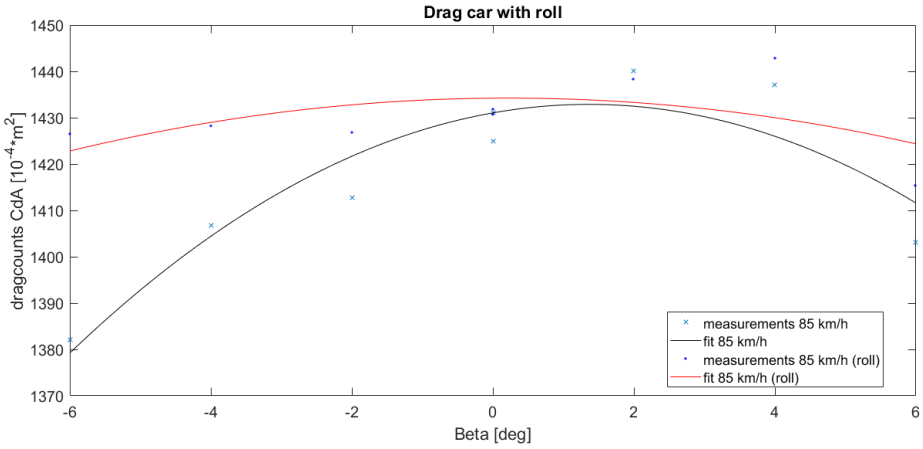

Figure 40: The dragcount comparison between no roll and 1.4º of roll angle at 85 km/h

The electrical engineers wanted to be able to orient the solar array to the sun as much as they could. From an electrical point of view, it is beneficial to orient the solar cell array perpendicular to the sun. One of the possibilities explored in the windtunnel was differential ride height (independent left and right ride height). This would allow us to roll the car while driving, better orienting the array to the sun. Before this

could be carried out, a test had to be conducted to analyze the drag penalty incurred by rolling the car during driving.

It can clearly be seen that there is a significant drag penalty when even a very small roll angle of 1.4° is used (Figure 39, 40). The drag penalty is acceptable for 0 degrees of yaw, but it increases rapidly for increasing yaw angles. Since in real life conditions the chances of exact head wind are very low, the drag penalty at higher yaw angles is a valid concern. The increase in solar power generation did not compensate for the drag penalty incurred by the yaw angle. This meant that using the adjustable spring damper system to increase the effectiveness of the solar array was scrapped.

Alpha sweep

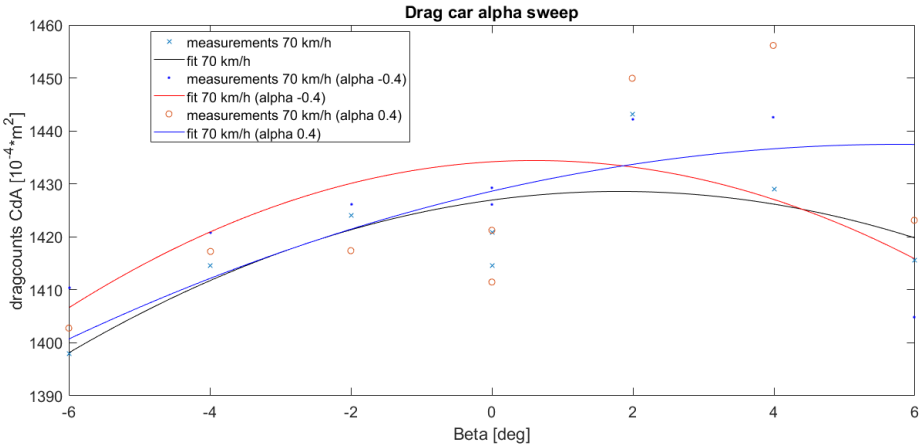

Figure 41: The results of the alpha sweep simulation

The alpha sweep (pitch angle) test was reduced to three angles due to time constraints. The final results were inconclusive (Figure 41). No clear difference could be seen between the different pitch angles, especially considering the relatively low accuracy of the balance used. Similar results could be seen for the test at the increased speed of 85 km/h.

Splitters

Figure 42: The splitters as they were eventually mounted onto RED Shift (seen behind the wheels).

The last test that was performed were the splitters (Figure 42). These were just simple plates of carbon fiber positioned behind the wheels. A simulation was performed using CFD with standing wheels, since doing simulations with rotating wheels was beyond the scope of the project at the time. These tests indicated a significant reduction in pressure drag. To verify the theoretical integration results, tests were conducted in the windtunnel (Figure 43.

In the windtunnel, similar effects on the total drag of the solar car were observed only at higher yaw angles. At zero yaw, no significant difference was observed. Still, also no negative effects were seen at zero yaw angle. The splitters were eventually used due to their seemingly positive effects during side wind conditions. It is impossible to determine the effect of the splitters with rotating wheels. Future teams will have to investigate their effects with a more advanced windtunnel setup and/or more advanced CFD simulations.

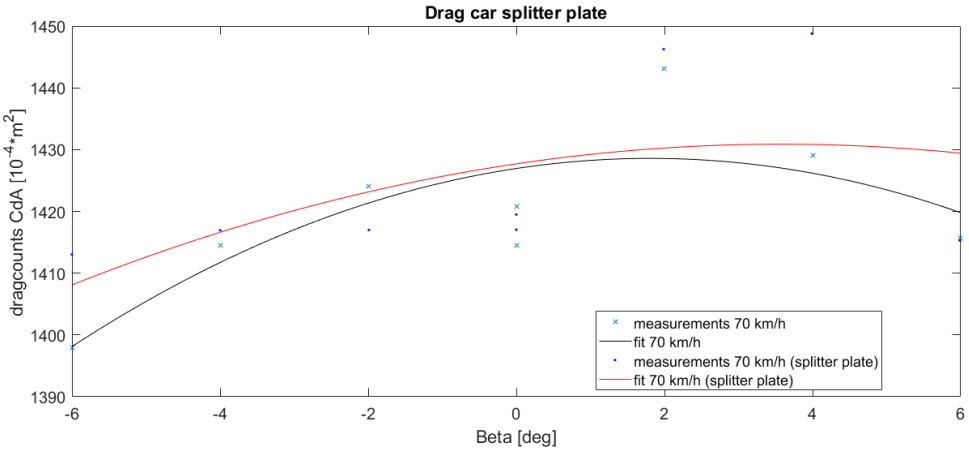

Figure 43: The difference in drag was observed mostly during higher yaw angles.

7. Banked road

The final step in estimating practical power figures was the banked road tests at RDW's test facilities (Figure 44a). Of course the CFD is a good tool to estimate the difference between different aerodynamic shell designs, but it gives a poor estimate for the total drag in the real world. It doesn't take surface roughness, split lines (for body panels), rotating wheels, production imperfections etc. into account. The validity of the CFD setup is also an important factor, but this was validated in the windtunnel.

The windtunnel does give a better estimate of the real drag figure, but the final figure is still not a good indicator of the drag due to several reasons. First of all the flow is conditioned as perfectly as it can be. As mentioned earlier the effects of a moving road and rolling tires is not taken into account and to make matters even worse the entire car was mounted on a giant splitter plate. This meant to comparative measurements were again quite accurate in the windtunnel, but absolute values were unreliable.

To obtain a better prediction of the real world power consumption of the car, Solar Team Twente always performs a number of final tests at RDW's banked road facility. In order to accurately obtain all the data necessary for a proper analysis a variety of system was used, which are listed in Table 6. Going into detail on each of these systems is far beyond the scope of this report, so it will be limited to a list of the hardware and the relevant measurements conducted.

Table 6: All measurements conducted during the banked road tests.

Hardware	**Measurement**	**Format**
Solar car DAQ	timestamp	UNIX timestamp in ms
	speed	m/s
	acceleration	m/s^2
	cruise	switch (1 or 2)
Weather sensors	wind direction	degrees
	wind speed	m/s
	air temperature	^oK
	barometric pressure	bar
Accelerometers	acc X/Y/Z	m/s^2
	gyr X/Y/Z	m/s
	roll/pitch/yaw	degrees
Calculated	car heading	degrees
	wind heading	degrees
	resultant velocity	m/s
	wind component	m/s

The coast down test

$$P = F \cdot v = \left(\frac{1}{2}\rho v^2 \cdot C_d A + mg \cdot C_{rr}\right) v \tag{13}$$

$$F \cdot v = m \cdot a \cdot v \rightarrow a = \underbrace{\frac{1}{2m}\rho C_d A}_{b_1} \cdot v^2 + \underbrace{mgC_{rr}}_{b_2} \tag{14}$$

A number of test were performed during the weekend. Only the coast down was relevant for the aerodynamic analysis of the car, so only this test is treated here. The basic premise of a coast down test is as follows: The car is accelerated to a constant speed (in this case to 110 km/h) after which the throttle and cruise control are turned off and the car simply coasts down. The velocity and deceleration are subsequently measured and plotted against each other in a scatter plot.

A quadratic fit is then created using Equation 14. From this fit the coefficients b_1 and b_2 are obtained. Subsequently, simple algebra the C_dA (aerodynamic drag area value) and C_{rr} (rolling resistance coefficient) are determined. From these values the Power consumption at each velocity was determined. To improve the accuracy of the data filtering and compensation techniques were used which will now be discussed.

Preparing the data

Test range identification

All measured data from both the solar car and the weather sensors is logged continuously and written to one large database. The data in this database is logged chronologically, but no further separation of the data is made. After extracting all data from the SQL databases, the accelerometer timestamp was used to extract the relevant ranges of data. The accelerometer saved its data per session, so its timestamp was an easy measure of both the start and the end of measurement sessions.

Corner compensation

Even though the banked corners are meant to simulate straight travel as much as possible. There will always be small lateral drag forces acting on the tires, resulting in inaccurate results. In order to prevent this from happening, the banked road was split into four zones, the two straights and the two corners. Shortly before entering and shortly after exiting the corner the cruise control would be enabled/disabled. The state of the cruise control could then be read from the car's Data Acquisition (DAQ) system. Whenever cruise was enabled, the data could be thrown out. This resulted in an even smaller data set, which in turn meant less computational time for the calculations.

Merging of data

The three different sources logged their data at different frequencies and there was also a slight offset in timestamp at the start of measurements. The highest frequency data source was used as a frequency baseline, after which the data was matched using the timestamp data available. Low frequency data obviously has less data points per given time interval than high frequency data. At the data points between two low frequency measurements, the data was interpolated to match the amount of high frequency data points. This could reliably be performed, because the low frequency data was not fast changing data (i.e. wind direction and air temperature).

Wind compensation

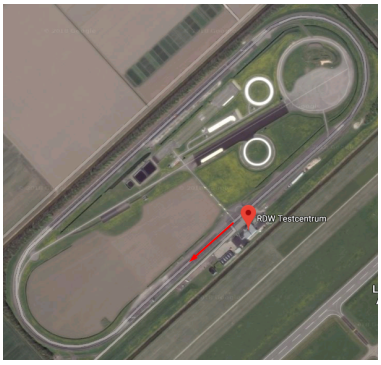

(a) The layout of the RDW test track. The red arrow represents the starting position.

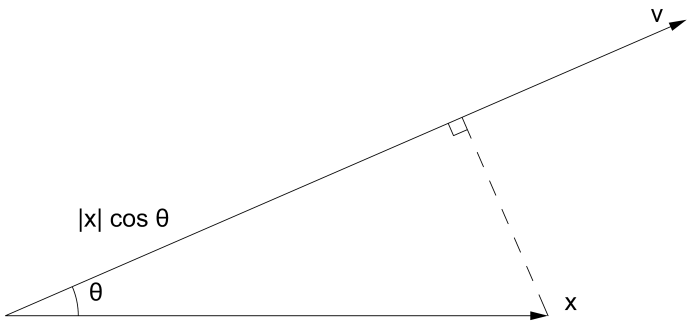

(b) The component of x on v is $comp_{\boldsymbol{v}}\boldsymbol{x} = |\boldsymbol{x}| \cos\theta$

Figure 44: The wind compensation approach.

An effort was made to compensate for wind present during testing. A tail- or head wind would obviously affect the deceleration being measured during the coast down procedure. The accelerometer was used

to obtain the yaw angle relative to the starting position of the solar car. A 0 degree yaw angle meant the car was present on the main straight, while a 180 degree yaw angle (approximately) meant that the car was on the back straight. From this information the car heading was determined, as the heading of the two straights was known.

As already mentioned in Table 6, the wind direction and the wind speed were being recorded during the tests. Using the wind direction, the wind heading was determined. After this, the head wind component of the wind velocity was determined using the approach shown in Figure 44b. For the compensation this velocity component (Figure 44) was directly subtracted (or added, in the case of a tail wind) from the velocity of the car itself.

In the end this approach was not completely satisfactory and there wasn't enough time to implement a more accurate, but more complicated approach. It was still used, as the wind corrected data was still an improvement over the original data, but a better wind correction and with it better C_dA estimation is something that should be looked into in the future.

Results

C_dA

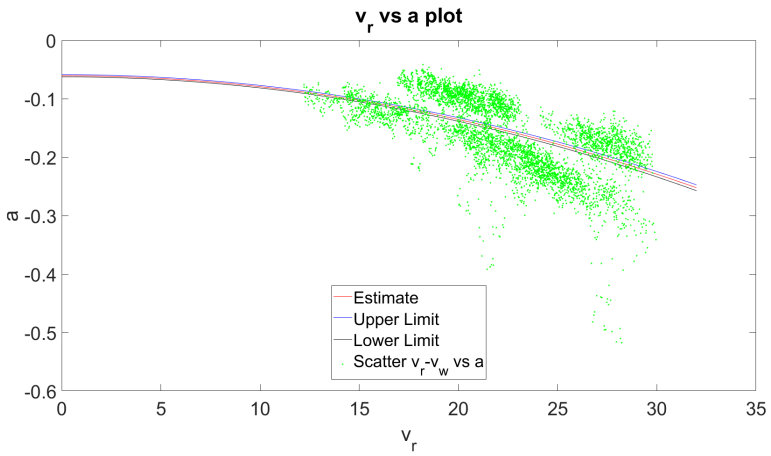

Figure 45: v_{car} scattered against a. Not corrected for wind effects

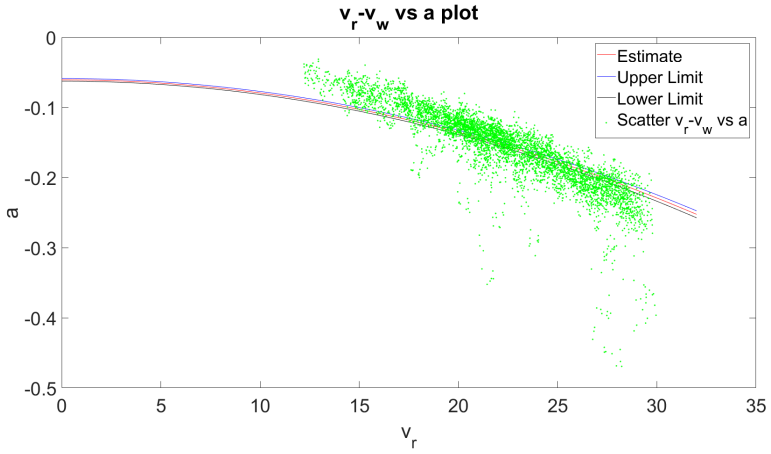

Figure 46: v_{car} scattered against a. Corrected for wind effects

The basic approach to estimating the C_dA value was already explained in Section 7.1. Figures 45 and 46 show the velocity scattered against the acceleration (or deceleration, in this case). In Figure 45 it can clearly be seen that two bands are present. The higher band represents the coast down

sessions conducted on the straight where a tail wind was present. This explains the lower than average deceleration (less negative). The opposite is true for the lower of the two bands. This band represents the straight where a head wind was present.

Figure 46 represents the wind corrected scatter of the velocity against the acceleration. A fit is made through both data sets which uses Equation 14. It is immediately obvious that the fit is not entirely accurate, since the deceleration is not zero at $v = 0$. The C_dA value was estimated to be 0.071 ± 0.001 with a confidence interval of 95%. This is most likely an underestimation of the actual value and a better approach is needed to estimate the real C_dA value for the solar car.

P vs v

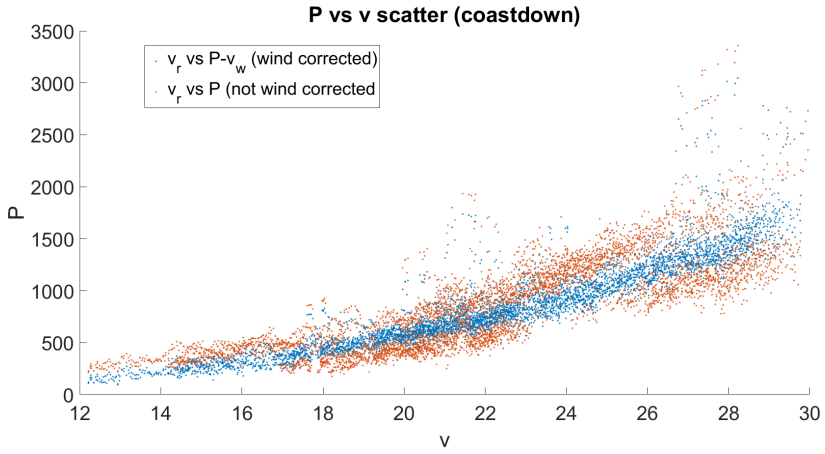

Figure 47: The Power requirement of the solar car as a function of the velocity. Without wind correction two clear bands can again be observed in the data.

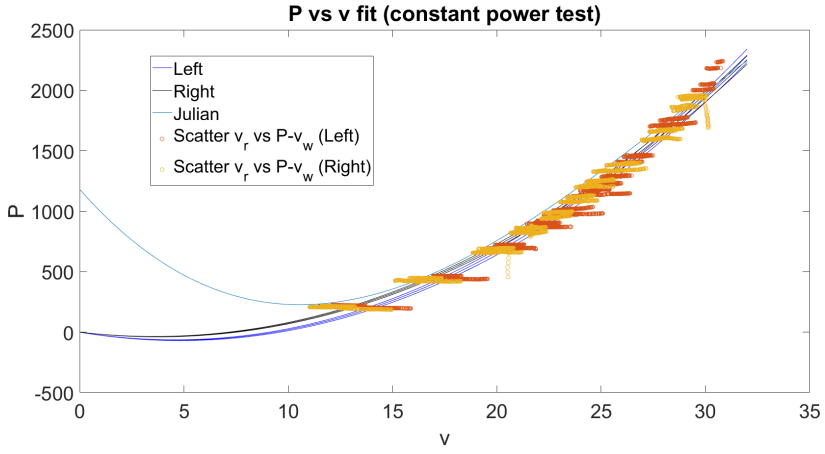

Figure 48: The final P vs v fit during one of the other tests. The *Left* and *Right* indicate the placement of the motor controller unit, which is irrelevant for the current discussion. *Julian* was 2015's P vs v fit. This fit proved to be perfectly accurate for race relevant velocity's.

One of the key strategy estimators is the power against velocity estimate. It allows the strategist to accurately estimate the expected power consumption of the solar car at any given time at any given velocity. It also allows him to plan the best course of action during a given race day.

Figure 47 shows the scatter of the power requirement against the velocity situation during a coast down test. Two bands are again clearly visible in the data when it is not corrected for head or tail wind. Equation 13 was used to obtain a fit through the data. Figure 48 shows that fit for a variety of scenario's.

This specific fit was not taken from a coast down test, but from a constant power test. Electrical losses were taken into account by doing so. All scattered data in this plot is already wind corrected.

The *Left* and *Right* in Figure 48 indicate the position of the motor controller unit (MCU). During the banked road tests it was still unsure where it would eventually placed, mainly because of the weight distribution in the car. It is not relevant for this discussion. The *Julian* line shows the power against velocity fit used by the 2015 team for their race strategy model. It is in agreement with the current fit for most of the velocity range but wildly diverges at low velocities. This was the main reason why a new attempt was made at improving the C_dA and power estimates.

Eventually the fits would prove to be a reliable estimator of the power consumption at different velocities. It is debatable if the proper formula was used to create the fit, because both the C_dA estimate and the C_{rr} estimate seemed to be unrealistically low. This is something that should be looked into by the 2019 team.

8. Recommendations

Design considerations

One of the key factors in the design of the solar car will always be the solar array. We do believe, like we have always done, that the gallium arsenide array is the better option. One of the key advises we can give to the new 2019 team is to design a solar car with a gallium arsenide array instead of a silicon array. Of course money is always a big issue and this is out of the aerodynamicists' control. Still, if at all possible financially, this is one of the key areas of improvement for the next team.

Switching solar arrays would of course mean a complete redesign of the solar car. But I am confident that the new team will be able to pull this off without much trouble. The aerodynamic knowledge of the new team combined with the knowledge of previous members should be more than enough to make this a rather trivial exercise.

If a choice is made for silicon, configuration studies will be key. The 2017 competitor is a good basis for this. Different track widths, wheel bases, main airfoil placements etc. should be tested. We are confident that the 2017 team spent too little time during this phase of the aerodynamic design of the car while spending too much time on the detailing of the whole car.

Theoretical design

One of the key possible improvements for the theoretical design of the solar car is an improvement in the analysis of the aerodynamic characteristics of the rotating wheels. Currently the effects of the rotating wheels is not taken into account, while it is presumed that they contribute a large amount of drag to the total drag of the solar car.

Setting up a proper isolated model for analyzing the effect in CFD will be key. It will allow the team to analyze the exact effects that the wheels have on the airflow around the car and subsequently they will be able to minimize the drag caused by them.

Windtunnel

The key recommendation regarding the windtunnel is again related to the rotating wheels. For many years now there has been talk about building a test rig which would be able to simulate a rolling tire on a rolling road. This would finally allow the team to verify the actual effects of the rotating wheels on the drag of the solar car as well as test possible measures to reduce this drag. Another aspect that could be tested here is wheel casings which entirely enclose the wheels. Other teams have been seen running these designs and it is an interesting concept to test.

Banked road

For the banked road tests possible improvements are two fold: First of all, the equation used for fitting the data should be reconsidered. If an equation can be derived which more accurately links aerodynamic drag, rolling resistance and perhaps even other factors to total power usage a much better prediction could be made of the actual C_dA of the solar car. The second component is the correction for the wind velocity. The current correction looks relatively accurate, but if a better model for correcting the presence of wind is available, this should be considered.

9. References

[1] *Bridgestone World Solar Challenge Organisation*. https://www.worldsolarchallenge.org/.

[2] BWSC *regulations*. https://www.worldsolarchallenge.org/files/1502_2017_bwsc_regulations_final_release_version_1.pdf.

[3] J. Hirschtick. *SolidWorks 2017*. d'Assault Systems, 2017.

[4] R. McNeel. *Rhinceros 3D 5.0*. McNeel, 2017.

[5] Eastman N Jacobs, Kenneth E Ward, and Robert M Pinkerton. "The characteristics of 78 related airfoil sections from tests in the variable-density wind tunnel". In: (1933).

[6] Eastman N Jacobs and Robert M Pinkerton. "Tests in the variable-density wind tunnel of related airfoils having the maximum camber unusually far forward". In: (1936).

[7] Laurence K Loftin Jr. "Theoretical and experimental data for a number of NACA 6A-series airfoil sections". In: (1946).

[8] Mark Drela. "XFOIL: An analysis and design system for low Reynolds number airfoils". In: *Low Reynolds number aerodynamics*. Springer, 1989, pp. 1–12.

[9] A Deperrois. "XFLR5: a tool for the design of airfoils, wings and planes operating at low Reynolds numbers". In: *Software Package* (2010).

[10] NA Chigier and VR Corsiglia. "Tip vortices: Velocity distributions". In: (1971).

[11] J. Swanson. *ANSYS 17.2*. ANSYS Inc., 2017.

[12] *ANSYS CFX-Pre Library Materials*. https://www.sharcnet.ca/Software/Ansys/16.2.3/en-us/help/cfx_mod/i1344110.html.

[13] Florian R Menter. "Review of the shear-stress transport turbulence model experience from an industrial perspective". In: *International Journal of Computational Fluid Dynamics* 23.4 (2009), pp. 305–316.

[14] Yi CHEN and Zheng-hong GAO. "Application of gamma-theta transition model to flows around airfoils [J]". In: *Acta Aerodynamica Sinica* 4 (2009), p. 005.

[15] Stephen B Pope. *Turbulent flows*. 2001.

[16] Takeo Kajishima and Kunihiko Taira. "Reynolds-Averaged Navier–Stokes Equations". In: *Computational Fluid Dynamics*. Springer, 2017, pp. 237–268.

[17] EA Spiegel and G Veronis. "On the Boussinesq approximation for a compressible fluid." In: *The Astrophysical Journal* 131 (1960), p. 442.

[18] *NASA: Isentropic flow, calorically perfect gas*. https://www.grc.nasa.gov/www/BGH/isentrop.html.

[19] Bryon D Anderson. "The physics of sailing". In: *Physics Today* 61.2 (2008), p. 38.

10. Appendix A - Description of employer and experience

Solar Team Twente

Solar Team Twente is a student team consisting of students from Saxion Hogeschool and Universiteit Twente. The students in this team design, built and test a solar car which takes part in the biennial Bridgestone World Solar Challenge. Although Twente has yet to win it's first world title, nowadays it is consistently amongst the top teams.

For the 2017 project 20 students took part in a variety of roles. These were broadly grouped into the technical team, management team and communications team. Within the technical team one of the sub teams was the aerodynamics team. This team was responsible for designing and testing a shell for the car which complied with the regulations, fit a driver and all mechanical, structural and electrical components while keeping the aerodynamic drag to a minimum.

My time at Solar Team Twente

Figure 49: The 2019 aerodynamics team, including Hans, at the windtunnel test.

Solar Team Twente is a group which is ambitious and efficient. When I applied for the position within the team I didn't quite realize how much work gets done in the incredibly short time a team gets to complete their goal. I still remember the first time we met Hans, where Hans told us: *Well, if we only have five months then we should really get a move on.* We hadn't yet mentioned to Hans that we only had five months to begin with.

I never directly applied for the aerodynamics function, and there is a good reason for that. I had never done a single thing with fluid dynamics in my life up until that point. When I applied I did so with an open application for a technical function in the team. In the end I was given an aerodynamics case and the rest is history. Not knowing much about fluid dynamics did make my time at Solar Team Twente much more challenging, though. Besides designing the car in five months, I also had to learn a lot about aerodynamics and fluid dynamics in general. I think it says a lot about the team that this was even possible. The amount of guidance from old team members and Hans, combined with the brilliant team members I was paired with is the only reason I was ever able to pull off my part of the design of the solar car in the first place. I have yet to meet another group of people who are so incredibly dedicated and I have to admit I miss it already.

On a personal level I think my time at Solar Team Twente has been one of the most influential times in my life. I have gained a lot of technical insights during my time there, but it pales in comparison to the amount of personal development I have gone through. I have learned a lot about working with

a varied group of individuals, including colleagues who are not engineers. I am now able to temper my expectations when starting out on new projects, without losing any of the ambition that has always been there. This also allows me to take rest when it is necessary and I'm better able to accept partially reaching my goals when fully reaching simply isn't realistic. It has been a year of big highs and big lows, but I wouldn't trade my experience at the team for anything, which I think will become a defining moment in my career as a mechanical engineer.

As a final footnote I would again like to thank Hans, without who this all wouldn't have been possible. In the end no matter how ambitious and talented we all are, we're frankly just a bunch of students. We do the very best we can, but we have no real experience to speak of and the entire process of designing the car is one big learning experience. Hans' vast amounts of experience in the field of aerodynamics have played an instrumental role in the success of the aerodynamic part of the project. From the theoretical design of the solar car where CFD played an important part to the more practical parts of the project like the windtunnel tests, Hans was always there to provide us with valuable knowledge and insights.

11. Appendix B - Evaluation

Added to this report as *EvaluationLBE.doc*.